Spatial restriction of phosphoinositide metabolism is a molecular switch to promote metastasis.

Marisa Nacke[1,2], Emma Sandilands[1,2,*], Konstantina Nikolatou[1,2,*], Álvaro Román-Fernández[1,2], Susan Mason[2], Rachana Patel[2], Sergio Lilla[2], Tamas Yelland[2], Lynn McGarry[2], Emma Shanks[2], Hing Leung[1,2], Sara Zanivan[1,2], Shehab Ismail[1,2], Elke Markert[2], Karen Blyth[1,2], David M. Bryant[1,2,3]

[1]Institute of Cancer Sciences, University of Glasgow and [2]The CRUK Beatson Institute, Glasgow G61 1BD, United Kingdom.

*These authors contributed equally.

[3]Correspondence: DMB (david.bryant@glasgow.ac.uk)

Abstract

The signalling pathways underpinning cell growth and invasion use overlapping components, yet how mutually exclusive cellular responses occur is unclear. We developed 3-Dimensional culture analyses to separately quantify growth and invasion. We identify that select *IQSEC1* variants, an ARF GTPase Exchange Factor, act as switches to promote invasion over growth by spatially restricting cortical phosphoinositide metabolism. All *IQSEC1* variants activate ARF5- and ARF6-dependent PIP5-kinase to promote PI(3,4,5)P_3-AKT signalling and growth. In contrast, select pro-invasive *IQSEC1* variants restrict cortical PI(3,4,5)P_3 production to discrete domains, resulting in formation of invasion-driving protrusions. Inhibition of *IQSEC1* attenuates invasion and metastasis *in vitro* and *in vivo*. *IQSEC1-ARF* expression predicts long-term outcome in prostate cancer patients. Spatial restriction of phosphoinositide metabolism therefore is a switch to induce invasion over growth in response to the same external signal. Targeting *IQSEC1* as the central regulator of this switch represents a therapeutic vulnerability to stop metastasis.

Highlights

- Spatial restriction of PI(3,4,5)P_3 is a molecular switch to promote invasion.
- IQSEC1 is a GEF for ARF5/6, promoting PIP5K-dependent PI(3,4,5)P_3 production downstream of the HGF receptor Met.
- Pro-invasive IQSEC1 variants restrict cortical PI(3,4,5)P_3 production to select cortical subdomains that convert into invasive protrusions.
- IQSEC1 inhibition attenuates in vitro invasion and metastasis *in vivo*.
- IQSEC1 module expression predicts disease-free survival in prostate cancer.

Keywords

IQSEC1, ARF GTPases, PIPs, Met, LRP1, Akt, 3D invasion, growth

Introduction

A central conundrum in biology is that highly overlapping signalling pathways regulate distinct biological outputs. For instance, activation of Receptor Tyrosine Kinases (RTKs), and their downstream effectors such as the MAPK-ERK and PI3K-Akt pathway, can induce either growth or invasion. Since the development of invasive features and the progressive loss of normal tissue organisation are hallmarks of tumour progression [1] understanding how cells decode their response to external signals has significant clinical implications.

Metastasis is the major cause of cancer-related death, increasingly recognised as a collective migration event. For a collection of epithelial cells to invade they must undergo rearrangement of normal apical-basal cellular polarisation to clusters or chains of cells lead by an invasive front. The use of 3-Dimensional (3D) culture systems, whereby epithelial cells are embedded in gels of extracellular matrix (ECM) to undergo collective morphogenesis, has illuminated the molecular mechanisms of collective cell polarisation [2-6]. Such polarity rearrangements can be achieved via altered membrane trafficking of morphogenesis-regulating proteins. For collective invasion to occur, signalling receptors, such as RTKs, must be directed to domains where a pro-invasive ligand is exposed. Some RTKs, such as the HGF receptor Met, require internalisation and endosomal localisation for full oncogenic signalling [7-9]. Additional membrane trafficking steps, such as recycling back to the cortex, can provide sustained signalling to effectors [10]. However, what controls whether such signals result in tumour growth versus the induction of collective invasion and metastasis remains unclear.

The ARF family of small GTPases (ARF1-6) are implicated in the membrane trafficking and signalling mechanism underpinning single cell invasion [11-16]. ARF GTPases have fundamental roles in vesicular transport by regulating assembly of coat complexes, lipid-modifying enzymes, and recruiting regulators of other GTPases onto membranes undergoing scission [17]. ARF6 in particular has been shown to play key roles in controlling internalisation and recycling of RTKs by acting in concert with a number of GTP Exchange Factors (GEFs) [18-21] and GTPase-Activating Proteins (GAPs) [22 23-26]. Accordingly, small molecule ARF GEF or GAP inhibitors have been used to control invasion *in vitro* and metastasis *in vivo* [23, 27-29].

Despite the core requirement for ARF GTPases in membrane trafficking steps controlling RTK signalling, it remains unclear how they could promote an invasion

response, rather than growth, from an RTK. Are particular ARF-regulated trafficking pathways induced in invasive cells, such as to enhance endocytic recycling and sustained RTK activation, to promote invasion over growth? Here, we describe that specific pro-invasive transcript variants of the ARF GEF IQSEC1 are upregulated in invasive prostate tumours. These alternate variant proteins act as scaffolds to restrict phosphoinositide metabolism to discrete cortical membrane domains that mature into the invasive protrusion fronts. We identify that IQSEC1 can be targeted to inhibit collective invasion *in vitro* and metastasis *in vivo*.

Results

Expression of the ARF GEF IQSEC1 is associated with poor clinical outcome.

We examined whether ARF GTPase expression was associated with the acquisition of invasive behaviours. We used 3D culture of prostate cancer cell lines to represent the transition from non-tumorigenic to highly metastatic (Fig 1A). Non-tumorigenic RWPE-1 cells [30] formed acini with a central lumen (Fig 1A,B). RWPE-2, an oncogenic *KRAS*-expressing RWPE-1 variant [30] formed lumen-lacking aggregates, some of which developed invasive cell chains (Fig 1B, white arrowheads). Bone metastasis-derived PC3 cells [31] grew as heterogeneous acini, variably forming round, locally spread, or spindle-shaped invasive cell chains (Fig 1C). Multiday live imaging revealed that invasive chains were derived from single cells that first formed spherical aggregates (growth phase) that initially protruded into matrix, then elongated into chains (Fig 1C, arrowheads, invasion phase).

ARF GTPases function with GEFs and GAPs that control their GDP-GTP state cycling (Fig 1D) [17]. We observed several lines of evidence indicating an association of the GEF *IQSEC1* (also called *BRAG2/GEP100,* [32] with prostate tumorigenesis. ARF GTPases, and a number of ARF GEFs were robustly upregulated in PC3 (Fig 1E, F). *IQSEC1*, including multiple isoforms, was the most robustly induced GEF in RWPE-2 and PC3. Normal prostate expressed low levels of *IQSEC1*, while invasive lines (PC3, VCaP) had robustly upregulated *IQSEC1* mRNA, with little variation in copy number (Fig 1G). Western blotting of Androgen Receptor (AR)-proficient and -deficient prostate lines confirmed similar upregulation of ARF6 and IQSEC1 protein expression in metastatic prostate cancer cell lines (LNCaP, VCaP, DU145, PC3) (Fig 1H). *IQSEC1* mRNA expression was elevated in primary human prostate tumour tissue compared to normal prostate (Fig 1I). Low expression of *IQSEC1* in primary tumours from patients predicted an increased multi-year survival (Fig 1J). In contrast, although *IQSEC2* expression was elevated in PC3 cells, *IQSEC2* did not show a similar normal-to-tumorigenic spread across cell lines, was significantly lower in prostate tumours than normal prostate, and was unable to stratify patient outcome (Fig S1A-D). We thus focused on dissecting IQSEC1 molecular function.

IQSEC1 is a regulator of collective cell invasion.

We examined the potential contribution of IQSEC1 to cell growth and movement. Publicly available *IQSEC1* transcript information (Genbank, ENSEMBL) revealed multiple variants occurring through combinatorial use of alternate translational initiation sites and alternate splicing (Fig 2A). Western blotting suggested simultaneous expression of multiple variants in PC3 cells, with three IQSEC1 bands depleted by IQSEC1 shRNAs (Fig S1E). IQSEC1 depletion reduced proliferation proportional to knockdown efficiency (Fig S1E, F). As PC3 cells grow as a mixed morphology 3D culture (Fig 1C), we developed a machine learning approach to determine whether this heterogeneity also occurred in 2D (Fig S1G). Mirroring 3D (Fig 1C), 2D PC3 cells could be classified into round (54%), spread (21%) and spindle phenotypes (17%) (Fig S1H, I). IQSEC1 depletion selectively abolished spindle characteristics, causing increased spread behaviours (Fig S1J).

We examined whether IQSEC1-dependent spindle shape was required for cell movement. Live imaging of wounded 2D monolayers revealed cells of various shapes rapidly move into the wound (Fig S1K). IQSEC1-depleted cells displayed a modest defect in migration. In contrast, in 3D invasion assays, wounded monolayers embedded in ECM (Matrigel) invade by forming spindle-shaped protrusions that develop into multicellular chains (Fig S1L, white arrowheads). In IQSEC1-depleted cells, although some protrusions formed, multicellular chain formation and invasive activity was strongly compromised (Fig S1L, M). Thus, IQSEC1 is required for growth and multicellular invasive chain formation, resulting in defects in morphogenesis where cell elongation is required (Fig S1N).

IQSEC1 is a regulator of 3D acini invasion.

We dissected IQSEC1 contribution to growth and/or invasion in 3D PC3 acini, which can form without (round) or with (spindle) invasive characteristics (Fig 1C). We developed an automated method to quantify such growth versus invasive behaviour from hourly imaging of hundreds to thousands of 3D acini over multiple days (see Materials and Methods and Fig S2A).

Elevated IQSEC1 expression in PC3, compared to RWPE-1, was maintained upon plating of both cell types into 3D culture (Fig 2B). Growth of acini from single cells could be measured by increased Area over time (Fig S2B, C). The progressive development of protrusive invasion could be determined using a ‘Compactness’ measurement (Fig S2B, C, S1 and S2 Movies). Similar to 2D, IQSEC1 depletion

modestly decreased 3D acinar growth (Fig S2C), proportional to depletion levels (Fig S1E). Mirroring 3D wound invasion defects (Fig S1L), the most prominent effect of IQSEC1 depletion was abolished protrusive invasion (Fig S2B, C).

We examined whether protrusion-forming activity was a common feature of all IQSEC1 isoforms. We focused on the four annotated variants (v1-4; Fig 2A). IQSEC1 v1-4 possess the IQSEC family-defining features of a calmodulin-binding IQ domain, a catalytic SEC7 ARF GEF domain, and a lipid-binding PH domain. Alternate initiation sites provide v1 or v2 with unique N-termini, followed by a common N-terminal extension. Three variable C-termini can occur, with the v4-type tail truncating a potential nuclear localisation sequence.

Stable expression of all RNAi-resistant GFP-tagged IQSEC1 variants could restore growth and invasion to endogenous IQSEC1-depleted cells, to levels matching or above control cells (Fig 2C-F). Variants containing the N-terminal extension (v1, v2) conferred the strongest effect on growth. In contrast, protrusive activity occurred in an isoform-selective manner: only v2 restored spindle behaviours in both 2D and 3D, to levels surpassing controls (Fig 2E, F, S2D). Thus, IQSEC1 v2 (also known as BRAG2b) is a major regulator of 3D growth and invasion.

We explored the IQSEC1 v2 properties that promote invasion. IQSEC1 can function in ARF GTPase-dependent endocytosis at the cell cortex, and in the nucleus to control nucleolar architecture [32, 33]. V3 showed predominantly nuclear localisation, while v4 was cortical (Fig 2G, S2E). V1 showed mixed cortical and cytoplasmic localisation. In contrast, v2 appeared mostly cytoplasmic (Fig 2G, green arrowheads, S2E). We reasoned that in overexpressed GFP-tagged variants cytoplasmic localization may mask vesicular pools. Accordingly, a v2-specific antibody (Fig 2H) labelled endogenous IQSEC1 v2 in tubulovesicular compartments behind the tips of an invasive acinar protrusions in 3D (Fig 2I, J, arrowheads). Thus, IQSEC1 v2 functions focally at endosomes in protrusion tips (Fig 2I-J).

We mapped the domains of v2 responsible for its localisation and potent invasion-inducing activity. We reasoned this was conferred by the unique v2 N-terminus. However, using mutants and chimeras of IQSEC1 isoforms revealed a nuanced and combinatorial effect of alternate N- and C-termini on IQSEC1 localisation and protrusion-induction (Fig S2F-L). Surprisingly, the unique v2 N-terminus (2N) was not required for invasion. Any variant containing the v2-tail and *any* N-terminal extension promoted invasion. Replacing the unique v2 N-terminus

(2N) with that from v1 (1N) enhanced invasion over and above that of v2 (Fig S2J-L). This was concomitant with a shift away from nuclear or cortical localisation, towards the cytoplasm (Fig S2H, 1N/2C chimera). This is in contrast to v1 alone which did not induce invasion (Fig 2F). The presence of a v1-type C-terminus (1C) inhibits invasion, concomitant with a more general cortical recruitment. Presence of a v2 tail without N-terminal extension (i.e. v3) does not promote invasion. This maps the invasion-inducing activity of IQSEC1 to the N-terminal extension common to only v1 and v2. The type of C-terminus influences whether this N-terminus induces invasion (Fig S2F-L). Mutational inactivation of GEF activity (IQSEC1 v2^{GEF*}) confirmed that IQSEC1 v2-induced spindle shape in 2D (Fig S2G) and protrusive invasion in 3D (Fig S2I-L) are due to its ability to activate ARF GTPases. Thus, the N-terminal common extension in v2 confers enhanced invasive activity in a GEF-dependent manner.

IQSEC1 activates ARF5/6 in distinct locations within protrusions.

IQSEC1 functions with both ARF5 and ARF6 to control integrin endocytosis [13, 34]. Given IQSEC1 GEF activity-dependency for invasion (Fig S2I-L), we examined whether ARF5 and ARF6 are required for this process. While individual ARF depletion caused some changes that mimicked IQSEC1 loss, only combined ARF5/6 depletion reduced all aspects of 2D spindle shape, and 3D growth and invasion (Fig 3A-C, S3A). We examined whether individual or co-overexpression (OX) of ARF5 or ARF6, wild-type (WT) or fast-cycling mutants (Fig S3B, C) [13, 35], induced invasive behaviours. Only ARF5/6 WT co-overexpression increased 2D spindle shape, 3D growth and 3D invasion (Fig 3D-F, S3D-G). While fast-cycling mutants induced some 2D spindle behaviours, they failed to induce 3D effects, either alone or in combination, indicating that normal GTPase cycling was required. Crucially, IQSEC1 depletion abolished all effects of ARF5/6 co-overexpression (Fig 3D-F, S3H). This identifies IQSEC1 as the major GEF regulating growth and invasion with ARF5/6 as its major targets.

Despite identifying IQSEC1 GEF activity as essential for growth and invasion (Fig S2J-K) we did not observe global defects in GTP-loading of ARF5 or ARF6 upon IQSEC1 depletion (Fig S3I). As IQSEC1 v2 localised to a discrete pool at tips of protrusions (Fig 2J), we reasoned that IQSEC1 may regulate a small, but crucial, ARF5/6 pool. We developed an imaging-based approach to determine the

localization of the IQSEC1-ARF complex. Endogenous IQSEC1 v2 localised with ARF5-mNeonGreen and ARF6-TagRFPT in tubulovesicular structures near the leading edge lamellipodium of spindle 2D cells (Fig 3G, white arrowheads). In 3D, ARF5 displayed a prominent vesicular localisation in the cyst body, which overlapped with IQSEC1 in some regions, while ARF6 was prominent at cell-cell contacts lacking IQSEC1 (Fig 3H, yellow arrowheads and white arrows respectively). Both ARF5 and ARF6 could be found with IQSEC1 v2 in protrusion tips (Fig 3H, white arrowheads).

To identify the location of active ARF we expressed a sensor that detects GTP-loaded ARF proteins (GGA1 NGAT domain [36]) (Fig 3I). GGA1 NGAT-TagRFPT colocalized with ARF6 most notably in the tips of protrusions (Fig 3J, green arrowheads), and with ARF5 in puncta in the body of the protrusion (white arrowheads) and the cyst body itself (white arrows).

To confirm that IQSEC1 was controlling this localized GTP loading of ARF5/6 we developed an automated method to analyse the percentage of overlap of the GGA1-NGAT probe with ARF5- or ARF6-positive puncta. We validated the sensitivity of this approach by first examining whether chemical inactivation of ARF GEF or GAP activity could be detected (Fig 3I). We identified that a reported IQSEC1-ARF6 inhibitor (NAV-2729) [29], but not the Cytohesin family ARF GEF inhibitor (Secin-H3) [37, 38], also reduces IQSEC1-catalysed nucleotide exchange on ARF5 (Fig S3J, K). In cells, NAV-2729 significantly decreased GGA1-NGAT recruitment to both ARF5 and ARF6-positive puncta (Fig 3K, L). In contrast, the ARF GAP inhibitor QS11 significantly increased GGA1-NGAT recruitment to ARF6, while decreasing recruitment to ARF5. Thus, our approach sensitively detects GTP-loading of specific ARF subpopulations (Fig 3J, L). In IQSEC1-depleted cells we observed a robust decrease, but not complete loss, of recruitment of GGA1-NGAT to both ARF5 and ARF6 (Fig 3J, K). These data confirmed that IQSEC1 controls GTP loading of a pool of ARF5/6 that is crucial for invasive activity (Fig 3M).

We determined the morphogenetic effect of modulating ARF activity. Secin-H3 treatment, which minimally acts on IQSEC1-mediated ARF activation (Fig S3K) modestly decreased 3D growth, without affecting invasion (Fig S3L-O). ARFGAP inhibition (QS11) [27, 38] increased 3D invasion, without affecting growth. However, in line with being a dual IQSEC1-ARF5/6 inhibitor, NAV-2729 treatment abolished 3D growth and invasion. Thus, ARF5 and ARF6 are the major targets of IQSEC1 GEF

activity. Chemical inhibition of IQSEC1-directed ARF activation strongly attenuates 3D growth and invasion.

IQSEC1 is a scaffold for Met and Akt signalling.

All IQSEC1 variants possess the SEC7-PH domains required to activate ARF GTP loading (Fig 4A). The enhanced invasion-promoting capabilities of IQSEC1 v2 are conferred by the shared N-terminal extension (encoded by Exon 3; Fig 4A). We used mass spectrometry protein-protein interaction analysis of IQSEC1 chimeras to identify domain-specific IQSEC1 binding partners. We classified interactors as unique to v1 or v2 N-termini (1N or 2N), shared between v1 or v2 N-terminal extension (Exon 3), to the core IQ-SEC7-PH region (Core), or specific to the v2 C-terminus (2C) (Fig 4A). We prioritised interactors where multiple components of a complex could be identified. We ordered these by mRNA expression change from two pairs of PC3-derived sublines which possess epithelioid (PC3E, Epi) compared to mesenchymal properties (GS689.Li, EMT14) [39 40], to focus on invasion regulators (Fig 4A-C). Using this approach, we identified the interaction of IQSEC1 with a number of oncogenic signalling pathways (mTORC2, RAF, NFkB), cytoskeletal and scaffolding complexes (Utrophin, 14-3-3), a phosphatase (PP6), and trafficking complexes (EARP, AP3/ARFGAP1). In addition to the known interactors Calmodulin-1/-2, we also identified three transmembrane receptors (Met, LRP1 and SORL1), and other factors (TUBB6, FHOD1). We confirmed a number of novel IQSEC1 interactors in independent immunoprecipitations, and interactor protein level alterations by western blotting of a series of PC3-derived sublines with varying invasive abilities (Fig 4D, S4A-C).

We initially focused on transmembrane interactors of IQSEC1. Of particular interest, IQSEC1 associated with Met, the receptor for HGF. This occurred through the core region, indicating that all IQSEC1 variants can potentially interact with Met (Fig 4D, E, S4A). In contrast, two proteins interacted only with the invasion-inducing regions of IQSEC1: LRP1 (Low density lipoprotein receptor-Related Protein 1) and SORL1 (Sortilin-Related Receptor 1), members of the LDL Receptor family (Fig 4D, E, S4A). LRP1 and SORL1 protein, however, displayed a mutually exclusive expression: LRP1 expression was elevated in invasive PC3 sublines (EMT14, GS689.Li), whereas SORL1 was associated with epithelial sublines (PC3E, Epi) and was anti-correlated with active pY1234/1235-Met (pMet) levels in cells (Fig S4B, C).

In addition, LRP1 and Met both localised to the tips of invasive protrusions in 3D (Fig 4F, G), and formed a complex irrespective of IQSEC1 expression levels (Fig S4D). These data suggest that LRP1 and Met form a complex in the tips of protrusions to which IQSEC1 associates to promote invasion.

Supporting the enrichment of active Met and LRP1 in invasive PC3 sublines (Fig S4A-C), depletion of LRP1 or Met reduced spindle shape in 2D and attenuated 3D growth and invasion (Fig 4H, I, S4E-G). LRP1 is a 600kDa protein that is cleaved to release a 515kDa extracellular fragment and an 85kDa transmembrane receptor [41, 42]. Expression of a GFP-tagged transmembrane LRP1 fragment (LRP1^{TM}-GFP) was not sufficient to induce invasion, suggesting both transmembrane and extracellular LRP1 fragments are required for invasion (Fig S4H). In contrast, SORL1 depletion increased spindle behaviours in 2D but did not significantly affect invasion or growth in 3D (Fig 4H-I, S4G, I-K). These data support a positive role for LRP1/Met in invasion, while SORL1 may be antagonistic; competing for the same binding site in IQSEC1 may be a mechanism.

We examined downstream signalling from Met that drives invasion. Although we identified RAF protein association with IQSEC1, MEK-ERK inhibitors minimally affected PC3 cell invasion (not shown). We thus focused on signalling to the TORC2-Akt pathway, as multiple subunits of this complex (RICTOR, SIN1/MAPKAP1, PRKDC) associated with IQSEC1. RICTOR is an essential positive regulator of mTORC2 [43, 44], while SIN1 has been reported to inhibit mTORC2 activity [45]. Accordingly, RICTOR depletion robustly abolished Akt S473 phosphorylation (pAkt), spindle shape in 2D, and 3D invasion and growth (Fig 4G-H, S4G, J-L). Notably, while SIN1 depletion decreased spindle behaviours in 2D, it robustly increased invasion in 3D, suggesting 3D-specific differences in this pathway (Fig 4H, I, S4G, M). Finally, we examined ARFGAP1 as a potential antagonist of IQSEC1-ARF function. Unexpectedly, ARFGAP1 depletion phenocopied IQSEC1 depletion: decreasing pAkt levels, spindle shape in 2D, modestly decreasing 3D growth, and profoundly inhibiting 3D invasion (Fig S4G, N-P). This suggests ARFGAP1 as an effector of ARF5/6 in regulating invasion and signalling to the mTORC2-Akt pathway (Fig S4Q), similar to observation of dual effector-terminator functions of other ARFGAPs [46-48]. Thus, an IQSEC1-ARF5/6-ARFGAP1 complex may control LRP1-Met signalling to mTORC2 during formation of invasive 3D protrusions.

An IQSEC1-LRP1 complex regulates Met endocytic trafficking.

Oncogenic Met signalling requires internalization [9]. We investigated whether IQSEC1 controls HGF-Met signalling to Akt by controlling Met endocytic trafficking. HGF stimulation increased 3D growth and robustly induced invasion, which was substantially blunted by IQSEC1 depletion (Fig S5C, D). ARF5/6 co-overexpression resulted in a modest but consistent increase in pAkt levels, which could be attenuated, but not abolished, in both control cells and HGF-stimulated cells by IQSEC1 depletion (Fig 3D, 5A,B, S5A, B). This suggests that despite 'active' pS473-Akt in cells, upon IQSEC1 perturbation, an invasive response was no longer possible.

IQSEC1-depleted cells displayed an increased half-life of Met (Fig S5E), suggesting delayed transit to degradative compartments. We examined whether this was due to altered endocytosis and/or recycling of Met (Fig 5C). We developed an image-based analysis of Met trafficking using a fluorescently conjugated anti-Met antibody (Fig 5C, D). This allowed dual quantitation of internalisation levels and localisation to cellular sub-regions (membrane, cytoplasm, juxtanuclear). In control cells Met was efficiently labelled at the cell surface, appeared in peripheral endosomes after 10 min internalisation, then clustered in the juxtanuclear region by 30 min (Fig 5D-F). IQSEC1-depleted cells showed a modest but significant delay in the internalisation and transit of Met from the periphery to the juxtanuclear region (Fig 5D-F), representing a strong decrease in total Met internalisation levels. We observed no significant difference in recycling of internalised Met (Fig 5E, 10 min), but defects in internalisation were re-apparent in extended time points of recycling that allowed for re-internalisation (30 min). Thus, IQSEC1 is required for efficient internalisation, but not recycling, of Met (Fig 5F).

We examined whether the positive (LRP1) and negative (SORL1) interactors of IQSEC1-regulated invasion we identified may also function by controlling activated Met trafficking. LRP1/SORL1 are regulators of endocytic sorting of a number of transmembrane proteins [49, 50]. In control cells, puncta containing activated Met (pY1234/5-Met, pMet) were distributed throughout the cytoplasm. Treatment with HGF induced a reduction in peripheral pMet puncta, concomitant with puncta clustering in the juxtanuclear region (Fig 5G-H), which was abolished by IQSEC1 depletion (Fig 5H-J). Consistent with a positive role for LRP1 in invasion, LRP1, but not SORL1, depletion also blocked redistribution of pMet away from the cell

periphery in response to HGF (Fig 5H-J). These data reveal that IQSEC1 and LRP1 control Met-induced invasion by regulating Met transport to the juxtanuclear region (Fig 5K), an essential function for signalling from Met [9].

IQSEC1-ARF signalling controls phosphoinositide generation in invasive protrusion tips.

We next examined how IQSEC1-ARF5/6 links Met to Akt activation. Generation of PI(3,4,5)P_3 (PIP_3) from PI(4,5)P_2 is an essential event in the Akt signalling cascade, allowing PIP_3-dependent recruitment of Akt to the cortex, PIP_3-dependent PDPK1 phosphorylation of Akt T308 [51] and the PIP_3-dependent release of SIN1 from RICTOR to allow Akt S473 phosphorylation [52]. PIP_3 generation requires the sequential action of PI4-kinases (PI4K), PIP5-kinases (PIP5K), and PI3-kinases (PI3K) to convert PI to PIP_3. All ARF GTPases can recruit and activate PIP5Ks [53-55], the latter of which there are three isoforms, PIP5K1A-C (PIP5K1$\alpha/\beta/\gamma$). ARF6 has been reported to activate PI3K signalling in melanoma [56] and to recruit PIP5K1α to Met [57]. We examined whether IQSEC1-ARF controls Akt activation by regulating PI(4,5)P_2 production as a precursor to PIP_3 generation (Fig 6A).

We examined cortical (vs. total) recruitment of biosensors to each lipid. Cortical PI(4,5)P_2 levels were not different between cell shape classes (spindle, spread, round) (Fig S6A, B). In contrast, cortical PIP_3 was elevated in both spindle and spread shapes, but with alternate distributions. Spread cells had uniform cortical PIP_3. Spindle cells displayed PIP_3 in the tips of protrusions in 2D and 3D (Fig S6A-D, 6B). Strikingly, cortical PI(4,5)P_2 levels were uniformly reduced irrespective of cell shape upon IQSEC1 depletion (S6A,B). Consequently, IQSEC1 depletion also decreased cortical PIP_3 levels in these cells, but not in the already low-cortical-PIP_3 round cells (Fig 6C, S6A, C). These data suggest that while IQSEC1-ARF-PIP5K controls general cortical PI(4,5)P_2 generation, the LRP1-Met-IQSEC1 v2 spatially restricts PIP_3 production to the tips of invasive protrusions (Fig 6A, S6D).

We examined the components of PIP_3 generation that drive invasion. Isotype-selective Class I PI3K inhibitors revealed that either PI3Kβ or PI3Kδ inhibition decreased pAkt levels, while PI3Kα or PI3Kγ inhibition paradoxically increased pAkt levels (Fig S6E). However, only PI3Kβ or Akt inhibition significantly attenuated 3D growth and invasion (Fig S6E-H). Depletion of PIP5K1A-C revealed that PIP5K1β

depletion showed the most robust decrease in growth, invasion, and pAkt levels (Fig S6G-I). These data suggest a PIP5K1β→PI3Kβ→Akt pathway for 3D growth and invasion.

Our data suggest that IQSEC1-ARF5/6 controls the PIP production and trafficking required for PIP5K1β→ PI3Kβ→ Akt signalling during invasion (Fig 6A). We tested whether generalised cortical targeting of this PIP-Akt pathway could overcome the need for IQSEC1 (Fig S6D). We targeted each of PIP5K1β, PI3Kβ, Akt1 to the cortex through addition of a myristoylation sequence, and inhibited IQSEC1 by shRNA or chemical means (NAV-2729) (Fig 6D-F).

Myristoylation of PI3Kβ (PI3Kβ^{myr}) or PIP5K1β (PIP5K1β^{myr}), but not PIP5K1α (PIP5K1α^{myr}), increased Akt phosphorylation, 3D growth and invasion, with the most robust increase occurring upon PI3Kβ^{myr} expression (Fig 6F, G). As expected in control cells, IQSEC1 depletion reduced pAkt levels and attenuated 3D growth and invasion (Fig 6E, F, G). Myristoylation of PI3Kβ (PI3Kβ^{myr}) or PIP5K1β (PIP5K1β^{myr}), but not PIP5K1α (PIP5K1α^{myr}), increased 3D growth and invasion with the most robust increase occurring upon PI3Kβ^{myr} expression (Fig 6E, G, H). Strikingly, IQSEC1 perturbation (shRNA, NAV-2729) had a disproportionate effect on invasion versus growth. While growth was blunted, in IQSEC1-perturbed conditions invasion was abolished (Fig 6E, G, H). NAV-2729 treatment blocked the ability of all cells in 3D to become acini. Single cells initially increased slightly in area and adopted irregular shapes, manifested in increased compactness, but not in invasion. Thus, generalized cortical recruitment of PIPK signalling is sufficient to drive growth, but not invasion; this requires IQSEC1-dependent restriction of signalling to invasion tips (Fig 6K).

IQSEC1-ARF regulates localization and activation of Akt.

Akt signalling showed a different influence on 3D behaviours than that observed for PI3Kβ or PIP5K1β. Our data suggest that IQSEC1 may contribute to Akt S473 levels by at least two mechanisms: influencing PIP5K1β-directed PI(4,5)P_2 production, and interaction with RICTOR-SIN1 (Fig 6A). While IQSEC1 depletion lowered endogenous pAkt levels, expression of myristoylated Akt1 (Akt1^{myr}) overcame the requirement of IQSEC1 for pS473 phosphorylation (Fig 6F, I, J).

Akt1^{myr} robustly increased 3D area at the expense of invasion compared to control cells (Fig 6I, J). Strikingly, although Akt1^{myr} no longer required IQSEC1 for phosphorylation events normally indicating 'activeness' (i.e. pS473-Akt; Fig 6F), IQSEC1 depletion still reversed the Akt1^{myr} -induced 3D growth increase to levels below control cells, and abolished invasion; NAV-2729 was similarly an inhibitor of these processes (Fig 6I, J). This suggests that IQSEC1 is required for Akt1-dependent signalling events over and above pS473 phosphorylation.

As experimentally 'active' Akt (Akt1^{myr}; as defined by pS473 levels) was unable to induce oncogenic signalling in IQSEC1-depleted cells we examined whether this was due to altered Akt localisation. In 2D, pAkt localised to cortical regions and to puncta distributed through the cytoplasm (Fig S6L). In 3D, a pool of pAkt was enriched in protrusion tips (Fig 6B, white arrowheads), as well as to puncta throughout the protrusion and acinus body. The global decrease in pAkt levels observed upon IQSEC1 depletion (Fig 5A) resulted from an amalgam of localisation changes; IQSEC1-depleted cells had a decrease of pAkt intensity on puncta in the juxtanuclear and cytoplasmic regions, concomitant with an increase in the size of pAkt puncta at the periphery (Fig S6K-M).

These data reveal that in addition to controlling PIP_3 generation for Akt activation, IQSEC1 controls the retrograde trafficking of Akt from the cortex to juxtanuclear endosomes for full signal output, similar to its influence on Met (Fig 5K).

IQSEC1 regulates growth and invasion *in vitro* and *in vivo*.

Our data indicate that LRP1-Met-IQSEC1 complex restriction of ARF5/6-dependent PIP_3 signalling to the tips of cellular protrusions induces invasion rather than growth. We tested the generalizability of IQSEC1 inhibition to inhibit growth and invasion mechanisms in commonly used prostate cancer models. mRNA expression (Cancer Cell Line Encyclopedia) and western blotting indicated that, with the exception of LRP1 in 22Rv1, all components of the LRP1-Met-IQSEC1-ARF5/6 pathway are expressed in examined prostate cancer cell lines (Fig S7A, B).

Inhibition of IQSEC1 by NAV-2729 attenuated growth and/or invasion in all 3D cancer cell models (Fig S7C-H). This included upon ectopic overexpression of endogenous LRP1-IQSEC1 complex lowly expressed proteins: the 85kDa cleaved transmembrane of LRP1 (LRP1^{TM}-GFP) in 22Rv1, or GFP-IQSEC1 v2 in DU145. DU145 grew as mixed morphology 3D cultures, displaying initially spherical acini

some of which progressed to spread locally. Treating with HGF changed the area and mode of invasion to resemble PC3, inducing elongating, spindle-type invasion (Fig S7D, H). This was abolished by NAV-2729 treatment (Fig S7D, H, I). Thus, IQSEC1 is required for growth and invasion across a number of 3D cell models.

We examined the *in vivo* role of IQSEC1 by intraprostatic xenograft of PC3 cells stably depleted of IQSEC1 (Fig 7A, B). While IQSEC1 depletion did not significantly attenuate tumour incidence, tumour area and volume were significantly reduced, indicating a defect in tumour growth (Fig 7C-E). Strikingly, metastatic activity was strongly decreased in IQSEC1-depleted cells. Both the incidence and number of macrometastases were significantly decreased in IQSEC1-depleted cells (Fig 7F, G). Wide-spread dissemination of macrometastases was observed in controls cells. In the few mice presenting macrometastases in IQSEC1-depleted cells, these were limited to prostate proximal lymph nodes (with the exception of a singular diaphragm-located tumour) (Fig 7H). These data indicate an essential requirement for IQSEC1 for growth and particularly invasion *in vivo*.

We examined whether expression levels of the IQSEC1-ARF module could further refine prediction of long-term prostate cancer patient outcome compared to IQSEC1 alone (Fig 1J). *ARF5* and *ARF6* expression were both elevated in primary human prostate tumour tissue compared to normal prostate (Fig 7I, J). *ARF5* levels were further increased in metastatic tumour tissue (Fig 7K, L). Examination of combined *IQSEC1*, *ARF5*, and *ARF6* expression in primary tumours robustly stratified the long-term biochemical disease-free survival outcomes for a cohort of 79 prostate cancer patients (GSE25136) (Fig 7M). This mirrored our *in vitro* results; low IQSEC1 expression was a highly favourable scenario, associating with low level of relapse, regardless of ARF expression level. Aligning with the elevation of ARF5 expression in metastases (Fig 7K), co-elevation of IQSEC1 and ARF5 could predict worst multi-year patient outcome and disease relapse.

Discussion

Our results clarify a long-held conundrum of how the same signalling pathways lead to distinct biological outputs: while a uniform cortical signal induces growth, spatially restricting phosphoinostide metabolism downstream of an RTK causes local remodelling of cortical subdomains into invasive protrusions.

We describe that IQSEC1 is a key node in the spatial restriction of PIP_3 signalling to promote invasion. Our data support a model whereby pro-invasive IQSEC1 isoforms form a complex with the HGF receptor Met and the endocytic receptor LRP1 at membranes that will develop into invasive protrusions (Fig 7N). IQSEC1 actives GTP loading on ARF6 to 1) stimulate PIP5K-mediated cortical $PI(4,5)P_2$ production, which is 2) a precursor to PI3K-mediated PIP_3 production to 3) promote invasive protrusion formation. Production of PIP_3 at invasive protrusions also triggers cell growth, concomitant with internalisation of Met and 4) activation of pAkt downstream of the mTORC2 complex. Met and pAkt are retrograde transported in the body of protrusions on ARF5 endosomes to a juxtanuclear signalling compartment, essential for growth and invasion. Inhibiting this IQSEC1-mediated ARF5/6 activation abolishes the collective growth and invasion/metastasis *in vitro* and *in vivo*.

Multiple isoforms of IQSEC1 exist through combination of alternate start sites and alternate splicing, though the regulators of these events are unknown. Such N- and C-terminal extensions operate in a hierarchy; N-terminal extensions provide association with endocytic co-receptors LRP1 and SORL1, while alternate C-termini can either positively or negatively enhance invasive activity. SORL1 and LRP1 are members of the LDLR family, co-receptors involved in endocytic control of a milieu of processes [41]. SORL1 and LRP1 shared the same N-termini binding region, were anti-correlated in their expression between invasive and non-invasive cells, and possessed antagonistic effects on invasion. This supports a notion that the function of IQSEC1 is highly contextual, dependent on not only which IQSEC1 transcript is expressed, but also the repertoire of potentially competitive interactors expressed.

LRP1 is a multifunctional endocytic receptor involved in a number of biological functions [41]. We report this as a crucial pro-invasive partner of IQSEC1 and Met. Endogenous LRP1 and Met were found in a complex irrespective of IQSEC1, suggesting that IQSEC1 binds an existing complex to couple their endocytic itinerary. This likely also requires the function of the extracellular cleaved 515kDa fragment of LRP1, as the transmembrane fragment alone is insufficient to drive invasion when expressed ectopically. LRP1 may help generate PIP_3 during invasion through its ability to form an LRP1-Rab8a:GTP-PI3K complex, to control Akt signalling on endosomes, as it does in other contexts [58].

Protrusive invasion requires a discrete pool of protrusive activity concomitant with global inactivity in surrounding regions, akin to pushing out from single point inside a balloon rather than simultaneously from all surfaces. IQSEC1 v2 localised with Met and LRP1 and coincided with PIP_3 production, at such a discrete event: the tips of invasive protrusions. Such exquisite spatial restriction coupled to invasive protrusion may explain why the most prominent cortically recruited IQSEC1 isoform (v4) fails to induce robust invasion, and perhaps why we see significant, but modest global GTP loading changes in ARF5/6 upon IQSEC1 depletion.

Why are both ARF5 and ARF6 required? Although ARF5 phenotypes most closely mimicked that of IQSEC1, there was still a dependency on ARF6. ARFs can act in pairs [59], and our data suggests that ARF5/6 may act at sequential steps: ARF6 at the cortex, and ARF5 in endosomes. It is interesting to note that previously described fast-cycling mutants of either ARF [35] were unable to induce collective morphogenesis like WT ARFs, suggesting that precise control over GTP cycling is essential for collective invasion. Indeed, a key effector identified was ARFGAP1, which in our hands functioned as an effector rather than an antagonist of ARF signalling, similar to the dual effector terminator function described for other ARFGAPs [46-48]. That this GAP associates with the GEF supports the notion of tight control over GTP cycling. Whether ARF5/6 both, or separately, interact with the two identified effectors (ARFGAP1, PIP5K1β), is unclear.

Internalisation of Met is key to full oncogenic output [8, 9]. IQSEC1 is crucial for efficient internalisation and juxtanuclear trafficking of Met and its downstream component pAkt. The generation of PIP_3 is central to invasion and growth downstream of Met signalling, and this is achieved by IQSEC1-ARF5/6-PIP5K1β production of $PI(4,5)P_2$, which is converted to PIP_3. Notably, although Akt was required for growth and invasion, Akt itself did not promote invasion, only growth. This suggests that following PIP_3 generation the signal transduction event branches: Akt-dependent growth (which is essential to develop to the stage to make protrusions) and Akt-independent, PIP_3-dependent invasion. The identity of invasion-specific PIP_3 effectors remains to be demonstrated, but one likely candidate is Rac1, which is dependent on PIP_3 for activation [60].

The ARF GTPase-dependent recycling of Met promotes sustained ERK signalling required for migration in other cells [57, 61]. Met recycling was not perturbed

in IQSEC1-depleted cells, suggesting another ARFGEF may promote this function. The PI(4,5)P_2/PIP_3-dependent Cytohesin-1 ARFGEF is one candidate for this, as we note upregulation in PC3, and it is required downstream of Met for invasive activity in other cells [62]. Cytohesin-1 alternate splicing controls its recruitment to membranes by controlling differential affinity for PI(4,5)P_2 or PIP_3 [63, 64]. Such a GEF would likely act subsequently to IQSEC1-directed control of cortical PI(4,5)P_2 levels. Thus, IQSEC1 may sit at the top of a cascade of ARF GEFs controlling Met endocytosis, recycling, and signal output. This may explain why IQSEC1 inhibition alone can reverse ARF5/6 overexpression, despite co-expression of numerous ARFGEFs in PC3 cells.

A striking result is that although IQSEC1-ARF5/6 could be considered 'upstream' of PI(4,5)P_2, PIP_3, and Akt, inhibition of IQSEC1 nonetheless counteracts the experimental activation of this pathway at multiple levels. Our data suggests that this is due to IQSEC1 controlling the spatial restriction of these signals. Although Akt can be 'active', as defined by S473 Akt levels, pAkt is not trafficked efficiently to the juxtanuclear region in the absence of IQSEC1, and is unable to induce full oncogenic output. This suggests targeting mechanisms of spatial restriction of signalling pathways may be effective in inhibiting oncogenic signalling, as previously demonstrated for c-Met [8], and demonstrated here for IQSEC1 and the PIP_3-Akt pathway.

Critically, we demonstrate that IQSEC1 inhibition blocks growth and invasion in a number of *in vitro* 3D models, and tumour growth and metastasis *in vivo*. Expression of this IQSEC1-ARF module is predictive of long-term recurrence-free survival in prostate cancer patients. In conclusion, we identify a molecular mechanism that allows cells to determine whether to grow or invade in response to activation of an RTK: restrict signalling output, such as PIP_3 production, to cortical subdomains to convert these into invasive protrusion, over a generalised cortical PIP_3 production which will cause a growth response.

Methods

Cell culture

PC3 (ATCC), PC3 E-Cad+, TEM4-18, TEM2-5, GS689.Li, GS694.LAd, GS683.LALN, JD1203.Lu, GS672.Ug (M. Henry, University of Iowa), PC3-Epi and PC3-EMT (K. Pienta, Johns Hopkins School of Medicine) and LNCaP cells (H. Leung, Beatson Institute) were cultured in RPMI-1640 supplemented with 10% Fetal Bovine Serum (FBS) and 6mM L-glutamine. RWPE-1, RWPE-2, WPE-NB14 and CA-HPV-10 cell lines (ATCC) were grown in Keratinocyte Serum Free Media (K-SFM) supplemented with 50µg/ml Bovine Pituitary Extract (BPE) and 5ng/ml Epidermal Growth Factor (EGF). DU145 and VCaP cells (ATCC) were maintained in Minimum Essential Medium (MEM) and Dulbecco's Modified Eagle Medium (DMEM) respectively both supplemented with 10% FBS and 6mM L-glutamine. 22Rv1 cells (H. Leung, Beatson Institute) were grown in phenol free RPMI-1640 containing 10% charcoal stripped FBS and 6mM L-glutamine. HEK293-FT (Thermo Fisher Scientific) were cultured in DMEM with 10% FBS, 6mM L-glutamine and 0.1mM Non-Essential Amino Acids (NEAA) (all reagents from Life Technologies). Growth factors or inhibitors were added as follows; 50ng/ml Hepatocyte Growth Factor (HGF) (PeproTech), 10µM NAV-2729 (Glixx Laboratories), 10µM QS11 (Tocris), 100µM chloroquine (CST), 20µM SecinH3 (Tocris), 25µM cycloheximide (Sigma), 1µM LY-294002 (Merck), 1µM AZD8835 (AstraZeneca), 0.1µM AZD8186 (AstraZeneca), 1µM AS-6052-40 (Stratech), 1µM Cal-101 (Stratech), and 10µM AktII (Calbiochem) inhibitors. Cells were routinely checked for mycoplasma contamination. PC3, RWPE-1 and RWPE-2 cells were authenticated using short tandem repeat (STR) profiling.

Generation of stable cell lines

Cell lines were made by co-transfecting plasmids with lentiviral packaging vectors (VSVG and SPAX2) into packaging cells (HEK293-FT) using Lipofectamine 2000 (Thermo Fisher Scientific). Viral supernatants were collected; filtered using PES 0.45µm syringe filters (Starlab) to remove cell debris, and concentrated using Lenti-X Concentrator (Clontech) as per the manufacturer's instructions. Cells were then transduced with the lentivirus for 3 days before either FACS sorting or selection with 2.5µg/ml puromycin, 300µg/ml G418 (both Thermo Fisher Scientific), 10µg/ml blasticidin (InvivoGen) or 200µg/ml hygromycin (Merck). Stable knockdown of proteins was achieved using pLKO.1-puromycin, pLKO.1-hygromycin or pLKO.1-membrane tagged Venus (substituted for puromycin) lentiviral shRNA vectors. Sequences as follows: shScr (5'CCGCAGGTATGCACGCGT3'), IQSEC1 KD1

(5'GATCTATGAACGGATCCGTAA3'), IQSEC1 KD4 (5'CCAGTACCAGATGAACAAGAA3'), Arf 5_1 (5'GATGCAGTGCTGCTGGTATTT3'), Arf 6_3 (5'GCTCACATGGTTAACCTCTAA3'), LRP1_1 (5'GATGCCTATCTGGACTATATT3'), LRP1_2 (5'GATCCGTGTGAACCGCTTTAA3'), MET_2 (5'GTGTGTTGTATGGTCAATAAC3'), SORL1_1 (5'GCCCAGTTTGTCACAAGACAT3'), SORL1_2 (5'CCTATGCCATTGCTGTCTTTA3'), RICTOR_1 (5'ACTTGTGAAGAATCGTATCTTCTC3'), RICTOR_2 (5'GCAGCCTTGAACTGTTTAA3'), SIN1_2 (5'CTAAGCAATCACGACTATAAA3'), ARFGAP1_1 (5'GTGCAGGATGAGAACAACGTT3'), ARFGAP1_2 (5'GCCAGTTCACTACGC AGTATC3'), PIP5K1α (5'GCTTCCAGGATACTACATGAA3'), PIP5K1β (5'ACGACAGGCCTAC ACTCTATT3') and PIP5K1γ (5'CAACACGGTCTTTCGGAAGAA3').

GFP-IQSEC1 v2 and GST-GGA3-GAT were kind gifts from J. Casanova (University of Virginia). All RNAi resistant variants and chimeras were made by mutagenesis or sub-cloning using fragment synthesis (GeneArt). GFP ARFs were kinds gift from P. Melancon (University of Alberta) and alternate fluorescent tags and mutations generated by sub-cloning. EGFP-PH-GRP1 and EGFP-PH-PLCδ were described previously[65] and sub-cloned into mNeonGreen. Myr-FLAG-Cre Myr-FLAG-PIP5Kα, Myr-FLAG-PIP5Kβ, Myr-FLAG-PI3Kβ, Myr-Akt1 and RFP-GGA1-NGAT were purchased from Addgene. LRP1-EGFP was a kind gift from S. Kins (Technical University Kaiserslautern). Plasmids will be deposited at Addgene.

Live 3D culture and analysis

Culture of cell lines as 3D acini was adapted from previous protocols [5]. Briefly, single cell suspensions were made (1.5 x 10^4 cells per ml) in the appropriate medium supplemented with 2% Growth Factor Reduced Matrigel (GFRM; BD Biosciences). 150µl of this mix was plated per well in a 96 well ImageLock plate (Essen Biosciences) pre-coated with 10µl of GFRM for 15 minutes at 37°C. Plates were incubated at 37°C for 4 hours, then imaged using an IncuCyte® ZOOM (Essen BioScience). Images were taken every hour for 4 days at 2 positions per well using a 10x objective lens. Sample size (n) and replicate number are stated for each experiment in Figure Legends. Outlines of phase and GFP-positive (where appropriate) acini were generated using a custom pipeline in CellProfiler. A custom macro in Fiji software was then used to colour code images from each time point, progressively coloured along a blue-to-red rainbow timescale, and concatenate them into one image per 12-hour block to reduce data dimensionality of multiday imaging. Using CellProfiler, measurements such as Area and Compactness, which could reliably measure size and protrusiveness of 3D PC3 objects respectively, were

generated for each 12-hour block. Custom pipelines designed in KNIME Data Analytics Platform were then used to collate data from multiple experiments, normalise to controls, calculate Z-score and perform statistical analysis using one-way ANOVA. Normalised data and p-values are presented as heatmaps generated in PRISM 7 (GraphPad). Total number of acini quantified per condition is stated in each Figure Legend.

Fixed 3D acini culture and analysis

Acini were set up as described above in 8-well coverglass chamber slides (Nunc, LabTek-II) pre-coated with 60µl GFRM. After 3 days at 37°C acini were washed twice with PBS and fixed in 4% paraformaldehyde for 15 minutes. Samples were then blocked in PFS (0.7% fish skin gelatin/0.025% saponin/PBS) for 1 h at RT with gentle shaking and primary antibodies added overnight (1:100) at 4°C. After three washes in PFS, Alexa Fluor secondary antibodies (1:200), HCS CellMask™ Deep Red Stain (1:50000) or Hoechst (1:1000) (all Life Technologies) were added for 45 minutes at room temperature (RT). Samples were maintained in PBS, after 3 five minute washes in PBS, until imaging was carried out. Acini were imaged using a Zeiss 880 Laser Scanning Microscope with Airyscan. Images taken in super resolution mode on the Airyscan microscope were processed using the Zeiss proprietary ZEN software, exported as TIFF files and processed in Fiji. Antibodies used; Alexa Fluor 488, 568 or 647 phalloidin (Life Technologies), anti-IQSEC1 (Sigma, G4798), anti-IQSEC1 (Caltag-Medsystems PSI-8009), anti-LRP1 (Sigma L2295), anti-Met (CST 3127), anti-Met phospho 1234/1235 (CST 3077) and anti-Akt phospho S473 (CST 3787).

2D Fixation and Phenotype Analysis

Cells were plated on a 96 well plate (Greiner) for 48 hours prior to fixation and staining as described above for 3D acini. Samples were imaged using an Opera Phenix™ High Content analysis system and Harmony High-Content Imaging and Analysis Software (PerkinElmer) was used to perform machine learning.

For 2D morphology assays cells were classified as either spindle, spread or round phenotypes using Harmony software. A custom pipeline was generated using KNIME Data Analytics Platform to collate data, calculate the log2 fold change of

each phenotype over control and to calculate statistical significance using one-way ANOVA. In some cases the intensity of specific proteins in sub-cellular regions such as nucleus, cytoplasm and plasma membrane was also calculated and the data Z-score normalised. GraphPad Prism was then used to generate heatmaps showing the fold change and p-values (grayscale). Sample number (n) and number of cells imaged per experiment is stated in the appropriate Figure Legend.

Colocalization between mNeonGreen-tagged ARF5 or ARF6 and RFP-GGA1-NGAT was also quantified using Harmony High-Content Imaging and Analysis Software. mNeonGreen and RFP spots were detected and the % green spot area overlapping with red calculated per cell. n=2 with 4 replicates per condition with > 500 cells imaged per condition.

Phosphoinositide intensity was calculated using an adapted version of PAPI (Pipeline for semi-Automated Phosphoinositide Intensity analysis) described previously [65]. Briefly, cells expressing mNeonGreen-tagged PH domains specific to each PIP were stained for cortex (phalloidin), cytoplasm (CellMask), and nuclei (Hoechst) as described above. Combinations of these dyes were used to create subcellular regions and the relative PIP probe intensity per area per cell measured. Data are Z-score normalised. n=3 with 4 wells per condition per experiment with > 1,500 cells imaged per condition.

These pipelines were adapted to measure the spot intensity of anti-Akt phosho-S473 in either the juxtanuclear, cytoplasmic or peripheral region of each cell and of anti-Met phospho-Y1234/1235 at the periphery. Data were Z-score normalised. n=2 with 4 replicates per condition with > 4000 cells imaged. Mann-Whitney test was used to calculate p values for pAkt localization.

All data are presented in box and whiskers plots and p values calculated using one-way ANOVA (unless stated otherwise); n.s. = not significant, *$p \leq 0.05$, **$p \leq 0.01$, ***$p \leq 0.001$ and ****$p < 0.0001$.

Animal studies

Animal experiments were performed under the relevant UK Home Office Project Licence (70/8645) and carried out with ethical approval from the Beatson Institute for Cancer Research and the University of Glasgow under the Animal (Scientific Procedures) Act 1986 and the EU directive 2010.

7-week-old CD1-nude male mice were obtained from Charles River (UK). 5 x 10^6 PC3 cells stably expressing either Scr (12 mice) or IQSEC1 KD4 (10 mice) shRNA were surgically implanted into one of the anterior prostate lobes of each mouse [66]. The mice were continually assessed for signs of tumour development and humanely sacrificed at an 8-week timepoint when tumour burden became restrictive. Primary tumours were imaged and tumour area and volume measured using VevoLAB ultrasound equipment and software. Significance was calculated using Mann-Whitney, *$p \leq 0.05$. Percentage of mice with tumours or with proximal (lumber lymph nodes and epididymal fat pads) or distal (thoracic lymph nodes and lungs) metastases were calculated by gross observation. p values were determined using a Chi-squared test (with fisher's exact test) adjustment, n.s. = not significant, *$p \leq 0.05$.

Met uptake assay

Met uptake assays were performed using a fluorescently labelled Met-647 antibody (BD Biosciences) to assess the cells' ability to internalise and traffic Met. Cells plated on 5 x 96 well plates were equilibrated at 37°C for 1 hour in antibody binding medium (RPMI + 0.5% BSA + 1 M $CaCl_2$, pH 7.4). Cells were washed twice with ice-cold PBS, incubated with Met-647 conjugated antibody for 1 hour at 4°C (1:100) then washed again with PBS. One plate was fixed as described previously. Two plates were treated with HGF (50ng/µl) and chloroquine (100µM) diluted in pre-warmed medium for 10 or 30 minutes at 37°C. They were then acid stripped (washed three times at 4°C with 0.5M acetic acid, 0.5M NaCl in PBS) and fixed as previously described. The remaining two plates were incubated at 17°C with pre-warmed medium supplemented with HGF and chloroquine for 1 hour. Acid stripping was performed and plates maintained at 37°C without HGF or chloroquine for 10 min or 30 minutes prior to fixation. Cells were stained with Hoechst and phalloidin and imaged using the Opera Phenix™ High Content analysis system. Data are presented as line graphs that show normalised (Z-score) relative region intensities compared to

the intensity of the whole cell. Box and whiskers plot shows total normalised (Z-score) intensity throughout the cells. n=2 with between 100-500 cells examined per experiment. P values were calculated using Welch's t-test and are shown on each graph as follows; n.s. = not significant, **p≤ 0.01, ***p ≤0.001 and ****p< 0.0001.

Protein Purification

pET20b-6xHis-ARF5D17 or pGEX-5x-1-hGGA3 [VHS-GAT] were transformed into BL21 (DE3) pLysS bacteria (Promega). Single colonies were grown in lysogeny broth (LB) medium in appropriate antibiotics until OD_{600nm} of 0.3. Protein expression was induced using 200µM isopropyl β-D-1-thiogalactopyranoside (IPTG, Sigma). Bacterial cells were pelleted and resuspended in 20ml Buffer A (for His-tagged: 20mM Tris, 300mM NaCl, 5mM MgCl2, 150µ l BME; for GST-tagged: 20mM Tris, 150mM NaCl, 5mM MgCl2, 150µl BME) containing protease inhibitors. DNAse (Sigma) was added to the lysate. Bacteria were lysed by passing through a 20,000 psi-pressurised microfluidizer. Lysates were collected at 20,000 x *g* for 40 min at 4°C and soluble proteins in the supernatant were sterile filtered 5µm PVDF Membrane (Merck).

PCR products encoding human IQSEC1-SEC7-PH (residues 517-866 based on variant 2 numbering) WT and GEF-dead (E620K) were cloned into pEGFP-C1 fused with an N-terminal 12xHis tag followed by a 6x Glycine linker replacing the GFP sequence. HEK293 suspension cells were transfected with constructs using polyethylenimine (PEI, Sigma). HEK293 suspension cells were cultured at 37°C and 8% CO_2 and 120 rpm. Cells were collected after 4 days, resuspended in His-IQSEC1 Buffer A (40mM Tris 7.5 pH, 300mM NaCl, 5mM $MgCl_2$, 60µl β-mercaptoethanol, 25mM Imidozol) and sonicated. Soluble fraction was collected at 40 min, 21,000 x *g* at 4°C and sterile-filtered using a 0.45µm PVDF-membrane (Merck).

Soluble fractions were loaded onto an ÄKTA purification system (GE Healthcare) using an equilibrated HisTrap or GSTrap (both GE Healthcare) column. The protein containing fraction was loaded onto the column at 1ml/min. Proteins were eluted from columns using an imidozol gradient buffer (25–300mM) or glutathione elution buffer (150mM NaCl. 25mM Tris, 20mM Glutathion) for His-tagged or GST-tagged proteins, respectively. Protein containing fractions were concentrated (Amigon Ultra-

15 centrifuge filter) and gel purified on an appropriate size exclusion column (Superose-6 10-300 GL 24ml for His-tagged IQSEC1, S75 16-600 120ml for His-tagged ARF5, S200 16-600 120ml for GST-GGA3) in Gel Filtration (GF) buffer (20mM Tris, 150mM NaCl, 1mM DTT, 5mM $MgCl_2$). Fractions containing purified proteins were concentrated, snap frozen and stored at -80°C.

Fluorescent Polarisation Assay

Nucleotide exchange of ARF5 protein was examined by observing changes in fluorescent polarisation. 100µM recombinant ARF protein was incubated with 200µM mantGDP and 50mM EDTA in Gel Filtration Buffer (GF) (20mM Tris, 150mM NaCl, 1mm DTT) overnight at 18°C. 100mM $MgCl_2$ was added to stop the exchange reaction. A PD10 (GE Healthcare) desalting column was then washed with GF buffer containing 5mM $MgCl_2$, 500µl of sample added and then eluted with GF buffer. Protein concentration was determined using a Bradford assay as per manufacturers instructions. 20µM of GDP nucleotide and 2µM of GEF protein was sequentially added to 1µM ARF and polarisation changes measured with a Photon Multiplier Detection System (Photon International Technology). Excitation was set to 366 nm and emission to 450 nm. Inhibitors were added to the reaction prior to addition of GEF protein.

Proliferation Assay

PC3 cells were plated in a 96-well ImageLock plate, in triplicate for 24 hours. Imaging was carried out on IncuCyte® ZOOM each hour for 48 hours. Cell area per well was then measured using the IncuCyte® ZOOM analysis software. n=3 independent experiments with 3 replicates per condition. P-values (Student's t-test): **$p \leq 0.01$ and ****$p \leq 0.0001$.

Invasion and Migration Assays

ImageLock plates were coated with 10% GFRM diluted in medium overnight at 37°C. Cells were re-suspended in 100µl medium and plated for 4 hours at 37°C. The resultant monolayer was wounded using a wound making tool (Essen Biosciences), washed twice with medium to remove debris, and overlaid with either 50µl of 25% GFRM for invasion assays or 100µl medium for migration assays. After an hour at 37°C 100µl medium was added to invasion assays and plates imaged every hour for

4 days using the IncuCyte® ZOOM. Sample number (n) and replicate number are stated in the appropriate Figure Legend. Results are presented as Relative Wound Density (RWD) for each time point and for the time point at which the average RWD of the control samples is 50% (Tmax1/2). Values are mean ± s.d. P values were calculated using Student t-Test and are shown on each graph as follows; n.s. = not significant, *p≤0.05, **p≤ 0.01, ***p ≤0.001 and ****p< 0.0001.

Immunoblotting

Cells were plated for 24 hours prior to treatment with growth factors or inhibitors for a further 24 hours. Plates were washed twice with ice cold PBS then Lysis Buffer added for 15 minutes (50mM Tris-HCl, pH 7.4, 150mM NaCl, 0.5mM $MgCl_2$, 0.2mM EGTA, and 1% Triton X-100 with cOmplete protease inhibitor cocktail and PhosSTOP tablets (Roche). Cells were scraped and lysates clarified by centrifugation at 13,000 rpm at 4°C for 15 minutes. BCA Protein Assay kit (Pierce) was used to determine protein concentration. SDS-PAGE was then performed and proteins transferred to PVDF membranes using the iBlot 2 transfer system (Thermo Fisher Scientific). Membranes were incubated for an hour in Rockland blocking buffer (Rockland) and primary antibodies added overnight at 4°C (1:1000 unless stated otherwise). Antibodies used were as follows; anti-GAPDH (CST 2118 1:5000), anti-IQSEC1 (Sigma G4798), anti-IQSEC1 (Caltag-Medsystems PSI-8009), anti-GFP (Merck 000000011814460001), anti-LRP1 (Sigma L2295), anti-Met (CST 3127), anti-Met phospho 1234/1235 (CST 3077), anti-Akt (CST 2920), anti-Akt phospho S473 (CST 3787), anti-ARF1 (Novus Biologicals NB-110-85530), anti-ARF6 (Sigma A5230), ARF5 (Novus Biologicals H00000381-M01), anti-ARFGAP1 (Sigma HPA051019), anti-SORL1 (BD 611860), anti-Sin1 (CST 12860), anti-RICTOR (CST 2114), anti-PPC6 (Sigma HPA050940 1:250), anti-14-3-3ζ/Δ (CST 7413), anti-PIP5Ka (CST 9693) and PIP5Kb (Sigma K0767). After addition of appropriate secondary antibodies for 45 minutes, membranes were washed three times in TBST and imaged using a ChemiDoc Imager (BioRad) or Odyssey Imaging System (LI-COR Biosciences). Sample number (n) is stated in the appropriate Figure Legend and quantitation is shown as mean ± s.d. P values were calculated using Student t-test and are shown on each graph as follows; n.s. = not significant, *p≤0.05, **p≤ 0.01, ***p ≤0.001 and ****p< 0.0001. GAPDH was used as a loading

control for each immunoblot and a representative image for each sample set is shown where appropriate.

GFP Trap and Immunoprecipitation

Immune complexes were collected when 1mg of cell lysate was immunoprecipitated with 2µg of anti-Met antibody (CST 3127) overnight at 4°C with rotation. Anti-mouse agarose or mouse agarose (both Sigma) were added for 1 hour at 4^{0}C prior to 3 washes in Lysis Buffer. Samples were then separated by SDS–PAGE, transferred to a PVDF membrane and immunoblotted. Lysates from cells expressing GFP tagged proteins were immunoprecipitated using a GFP-Trap Kit (Chromotek) as per manufacturers instructions and immunoblotting performed as above. n=3 and quantitation is shown as mean ± s.d.

Mass Spectrometry

For Mass Spectrometry analysis agarose beads were resuspended in a 2M Urea and 100mM ammonium bicarbonate buffer and stored at -20°C. On-bead digestion was performed from the supernatants. Triplicate biological replicates were digested with Lys-C (Alpha Laboratories) and trypsin (Promega) on beads as previously described[67]. Tryptic peptides were separated on a 20cm fused silica emitter (New Objective) packed in house with reverse phase Reprosil Pur Basic 1.9µm (Dr Maisch GmbH) using an EASY-nLC 1200 (Thermo Fisher Scientific) coupled online to an Orbitrap Q-Exactive HF mass spectrometer (Thermo Fisher Scientific) via nanoelectrospray ion source (Thermo Fisher Scientific). For the full scan a resolution of 60,000 at 250Th was used. The top ten most intense ions in the full MS were isolated for fragmentation with a target of 50,000 ions at a resolution of 15,000 at 250Th. MS data acquisition were performed using the XCalibur software (Thermo Fisher Scientific). The MaxQuant software version 1.5.5.1[68] was used to process MS Raw files and searched with Andromeda search engine[69], querying UniProt [70]. Database was searched requiring specificity for trypsin cleavage and allowing maximum two missed cleavages. Methionine oxidation and N-terminal acetylation were specified as variable modifications, and Cysteine carbamidomethylation as fixed modification. The peptide and protein false discovery rate (FDR) was set to 1%. The common reverse and contaminant hits (as defined in MaxQuant output) were removed. Only protein groups identified with at least one uniquely assigned peptide

were used for quantification. For label-free quantitation, proteins quantified in all 3 replicates in at least one group, were measured according to the label-free quantitation algorithm available in MaxQuant [71]. Significantly enriched proteins were selected using a Welch t-test with a 5% FDR (permutation based). The mass spectrometry proteomics data have been deposited as partial submission to the ProteomeXchange Consortium via the PRIDE partner repository [72] with the dataset identifier PXD013810. Hits were prioritised based on fold change expression data mined from publicly available RNAseq data from PC3 sublines from published data sets (PC3E versus GS689.Li; SRS354082) and PC3-Epi versus PC3-EMT14; GSE48230 [39, 40].

GGA3 Pulldown

A pulldown assay was performed to examine GTP-loading of ARF proteins using the ARF-GTP-specific binding domain of GGA3. Cells were cultured for 48 hours then serum starved overnight. HGF in serum free medium was added for 30 minutes. Cells were then lysed on ice in pulldown-lysis buffer (50mM Tris, 100mM NaCl, 2mM MgCl2, 0.1% SDS, 0.5% Na-deoxycholate, 1% Triton X-100, 10% glycerol), syringed 5 times and centrifuged at 4°C 14,000*g* for 1 minute. Spin columns were equilibrated with 50µl of Glutathione Agarose resin and washed with pulldown-column wash buffer (1:1 pulldown-lysis buffer and 1xTBS). 80µg of GST-GGA3-GAT recombinant fusion protein was immobilised on the agarose resin by incubation at 4°C with gentle rocking for 1 hour. 1.5mg of lysate was added onto spin columns and incubated at 4°C for 2 hours with rocking. Unbound proteins were washed off the column with pulldown-wash buffer (50mM Tris, 100mM NaCl, 2mM MgCl2, 1% NP-40, 10% glycerol). 60µl of pulldown-elution buffer (10mM Glutathione in 1xTBS) was added to the spin column and incubated for 5 min at RT. Eluted protein was collected at 1,250*g* for 1 minute and samples were prepared for SDS-PAGE and western blotting as described above.

qPCR

RNA was extracted using an RNeasy kit (Qiagen) and reverse transcription of RNA performed using a High-Capacity cDNA Reverse Transcription Kit (Life Technologies) following the manufacturer's protocols. TaqMan qPCR was then

carried out as per manufacturer's instructions (Life Technologies). n = 3 technical replicates. Data were analysed using the Applied Biosystems 7500 Software v2.0.6 and the relative quantitation (RQ) was calculated using the comparative C_t ($\Delta\Delta C_t$) method. *ARF* and *ARFGEF* expression were detected using a custom qPCR primer panel. Details are available on request.

Acknowledgements

This work was supported by the following grants; D.M.B. NIH K99CA163535, M.N. CRUK (C596/A19481), K.N. CRUK (C7932/A25170), E.S., AR.-F, L.M. S.Z., and S.L. CRUK C596/A17196, E.M. CRUK A25142, S.I. and T.Y. CRUK (A19257). We would like to thank the Core Services and Advanced Technologies at the Cancer Research UK Beatson Institute, with particular thanks to the Beatson Advanced Imaging Resource and Molecular Technologies.

Author Contributions

M.N. and D.M.B designed experiments and analysed data. M.N., D.B., K.N., E.S., T.Y., AR.-F, R.P., and S.M. performed experiments and analysis. L.M. and E. Shanks helped with the development of high-throughput imaging and analysis. S.L. and S.Z. performed and analysed the proteomic experiments. T.Y. and S.I. guided protein purification and biochemistry. E.M. analysed patient data. S.M. and R.P. performed, while K.B. and H.L. guided, *in vivo* experiments. D.M.B, M.N. and E.S. wrote the manuscript. D.M.B. supervised the study. All authors discussed the study and commented on the manuscript.

Competing Interests statement

The authors declare no competing interests.

Figure Legends

Figure 1. Upregulation of IQSEC1 is associated with tumorigenesis.

(A) Schema, prostate cell lines forming non-invasive or invasive 3D acini in extracellular matrix (ECM).

(B) Cartoon, phenotype of typical RWPE-1 and RWPE-2 acini. Confocal (F-actin (red) and nuclei (blue)) and brightfield images show RWPE-1 and RWPE-2 acini at 120 hours. Arrowheads, protrusions. Scale bar, 20μm.

(C) Schema, PC3 acini form (grow) and invade (protrusions) through ECM over time. Phase contrast images of PC3 acini where higher magnification of boxed region at different time points is shown. Arrowheads, protrusions. Scale bar, 100μm.

(D) Cartoon, ARF GTPase cycle.

(E) Heatmap representation of mRNA expression. Data are normalized to RWPE-1 and presented as the log2-transformed fold change compared to the average of all values. Bar graphs summarise fold changes of *ARF* and *IQSEC* mRNA levels. n=3 technical replicates. Values, mean ± s.d. p-values (Student's t-test).

(F) Schema, elevated activation of ARF GTPases in PC3 cells by GEFs such as IQSEC1.

(G) Graph generated using RNAseq data from the Cancer Cell Line Encyclopedia (CCLE) comparing *IQSEC1* gene copy number and mRNA expression levels in multiple breast and prostate cancer and non-transformed cell lines.

(H) Western blot analysis of androgen receptor (AR) proficient or deficient prostate cell lines using anti-ARF1, ARF6, pan-IQSEC1 isoform and GAPDH (as sample control) antibodies.

(I) Quantitation of *IQSEC1* expression levels in either 52 normal or 487 tumour samples mined from The Cancer Genome Atlas (TCGA). Box-and-whiskers plot: 10–90 percentile; +, mean; dots, outliers; midline, median; boundaries, quartiles. p-values (one-way ANOVA).

(J) *IQSEC1* gene expression from 487 primary prostate tumours (TCGA) was evaluated for outcome prediction from (recurrence-free) survival data. Patient samples were clustered into quartiles based on normalized gene expression. Highest expression, red, lowest expression, blue. Heatmap shows clustering of expression values. p values (Logrank).

All p-values: *p≤0.05, **p≤0.01, ***p≤0.001 and ****p≤0.0001.

Figure 2. IQSEC1 isoforms differentially regulate collective invasion.

(A) Schema, domain structure of IQSEC1 variants (v) 1-4. All variants possess an IQ motif, SEC7 and PH domains. v1 and v2 contain N-terminal extensions. A nuclear localization signal (NLS) is present in v1-3, lost in v4. v2/v3 share a common C-terminus. Common domains shown in grey, unique domains indicated by colour; blue; v1, pink; v2 and v3, green; v4.

(B) Western blot in 2D and 3D using anti-IQSEC1 antibody. GAPDH is shown for IQSEC1 blot. Relative expression of all IQSEC1 bands normalised to 2D RWPE1 is shown. n=6 independent experiments. Values, mean ± s.d. p-values (Student's t-test), *p ≤0.05; n.s. not significant.

(C) Cartoon, isoform specific IQSEC1 functions were identified by comparing the growth and invasion of acini expressing different GFP-IQSEC1 variants upon depletion of endogenous *IQSEC1* (shRNA KD4).

(D) Western blot of PC3 cells expressing GFP or GFP-IQSEC1 v1-v4, and either Scr or *IQSEC1* KD4 shRNA using anti-IQSEC1, GFP and GAPDH antibodies. All antibodies used on same membrane. GAPDH is shown for IQSEC1 blot. Different exposures of IQSEC1 (long, short) are presented to demonstrate expression of all

variants. Upper and lower parts of same GFP blot are shown to demonstrate expression of GFP-IQSEC1 variants and GFP control respectively.

(E) Phase images of acini from cells described in D. GFP positive acini are outlined in yellow. Scale bars, 100μm.

(F) Quantitation of images shown in E. Heatmap shows area and compactness measurements as Z-score-normalised to control (+-+-) values (upper panels). p-values (one-way ANOVA): greyscale values as indicated (lower panels). n=3, 3 replicates/condition, 300-650 acini per condition.

(G) PC3 acini described in D were stained for F-actin and nuclei (black and magenta respectively in upper panels) after 4 days. Green arrowheads, protrusions. Scale bars, 20μm. Localisation of GFP-IQSEC1 can be appreciated from FIRE pseudo coloured Look Up Table (FIRE LUT) (middle panels). Magnified images of boxed regions are inset. Cartoon, localization of GFP-IQSEC1 variants in PC3 acini (lower panel).

(H) Western blot of PC3 cells expressing GFP or GFP-IQSEC1 v1-v4 using anti-IQSEC1 (specific for v2) and GAPDH antibodies. GAPDH is shown for IQSEC1 blot. Different exposures of GFP (long, short) are presented showing GFP-IQSEC1 proteins. Upper and lower parts of same GFP blot are shown to demonstrate expression of GFP-IQSEC1 variants and GFP control respectively.

(I) Schema, summary of the effect of *IQSEC1* KD and expression of GFP-IQSEC1 v2 on growth and protrusive ability of PC3 acini.

(J) Endogenous IQSEC1 v2 co-stained with F-actin (green and red respectively in merge). Magnified images of boxed region are shown. Red arrowhead indicates localisation at protrusion tip.

Figure 3. IQSEC1 activates ARF5/6 in distinct locations within protrusions.

(A) Western blot of PC3 cells expressing Scr, *ARF5* or *ARF6* shRNA, alone or together, using anti ARF5, ARF6 and GAPDH antibodies. GAPDH is shown for ARF6 blot. ARF intensity normalised to Scr is quantified. n=3 independent experiments. Values, mean ± s.d. p-values (one-way ANOVA).

(B) Phase images of PC3 acini described in A. Yellow outlines indicate shRNA (mVenus) positive acini. Scale bars, 100μm.

(C) Quantitation of images shown in B. Quantitation is shown for area and compactness measurements as Z-score-normalised values (upper heatmap). p-values (one-way ANOVA): greyscale values as indicated (lower heatmap). n=3, 5 replicates/condition, 2880 - 3188 acini quantified/condition. Cartoon, acini phenotype representative of each condition.

(D) Western blot of PC3 cells stably co-overexpressing (OX) mNeonGreen (mNG) and TagRFP-T (RFP) (Control) or ARF5-mNG and ARF6-RFP (ARF5/6), and either Scr or *IQSEC1* KD4 shRNA. Anti-IQSEC1, ARF5, ARF6 and GAPDH antibodies were used. Both endogenous and exogenous (OX) ARFs were detected. GAPDH is shown for ARF5 blot.

(E) Phase images of PC3 acini described in D. Scale bars, 100µm.

(F) Quantitation of images shown in E. n=2, 4 replicates/condition, 1,254 – 1,567 acini/condition.

(G) PC3 cells co-overexpressing ARF5-mNG and ARF6-RFP (ARF5/6 OX) were stained for IQSEC1 v2 and merged image of spindle shaped cell shown (left panel). Magnified images of boxed region are shown. White arrowheads indicate areas of colocalization. Scale bars, 20µm.

(H) PC3 acini expressing either ARF5-mNG or ARF6-mNG were stained for IQSEC1. Localisation of these proteins is shown using FIRE LUT. Yellow and white arrowheads, colocalization in juxtanuclear region and protrusive tips, respectively. White arrows, lack of colocalization. Scale bars, 5µm.

(I) Schema, GTPase cycle of ARF5 and ARF6, site of action of the IQSEC1-inhibiting molecules NAV-2729, the pan ARFGAP-inhibitor QS11, and GTP-loaded ARF detection by a GGA1-NGAT probe.

(J) PC3 acini expressing either ARF5-mNG or ARF6-mNG and GGA1-NGAT-RFP were fixed and FIRE LUT of maximum projections (upper panels) and a single Z-slice of boxed regions (lower panels) shown. White and green arrowheads, colocalization in protrusions, white arrows, colocalization in cell body. Scale bars, 10µm.

(K-L) PC3 cells expressing **(K)** ARF5-NG and GGA1-NGAT or **(L)** ARF6-NG and GGA1-NGAT were stably transfected with either Scr or *IQSEC1* KD4 shRNA. Cells were treated with NAV-2729 or QS11 for 24 hours prior to fixation. Quantitation of % overlap of ARF and ARF-GTP probe per cell is shown in box-and-whiskers plot: 10–90 percentile; +, mean; dots, outliers; midline, median; boundaries, quartiles. n=2, 3

replicates/condition with a minimum of 500 cells/condition. p-values (one-way ANOVA): *p≤0.05, **p≤0.01, ***p≤0.001 and ****p≤0.0001.

(M) Schema, different localization of IQSEC1 and active ARFs in protrusions is shown.

Figure 4. IQSEC1 is a scaffold for Met signalling. (A) Schematic, IQSEC1 chimeras and variants display distinct phenotypes in 3D culture. GFP-trap immunoprecipitation was performed on PC3 cells expressing these proteins followed by tryptic digestion "on-beads" and LC/MS/MS analysis. IQSEC1 domain-specific interactions were identified and sorted by mRNA expression compared in paired PC3 subclones.

(B) STRING network analysis of IQSEC1 binding partners identified by MS visualized using Cytoscape. Most IQSEC1 binding partners could be clustered into 8 protein complexes (colour coded).

(C) Schema, indicates the protein complex each binding partner is associated with. Heatmap shows the fold change of IQSEC1 interactors from panel B binding to different IQSEC1 domains over GFP control. Values are $-\log_2(FC)$, very high = -7 to -5, high = -5 to -2.5, medium -2.5 to -1, low = -1 to -0.05, no binding >0.05. p-values are indicated in grey heatmap. The specific IQSEC1 domain to which each interactor binds is also depicted. Interactions were sorted according to the fold change in mRNA of non-invasive PC3 subclones (GS689.Li, EMT) compared to invasive subclones (PC3E, Epi) (RNAseq).

(D) GFP-trap immunoprecipitation was performed on PC3 cells expressing GFP, GFP-IQSEC1 v2 or v4. Western blot analysis was then carried out using anti-Met, LRP1, GFP, IQSEC1 and GAPDH antibodies. GAPDH is shown for LRP1 blot. Quantitation of LRP1/IQSEC1 and Met/IQSEC1 interactions for each GFP-trap are shown. n=3 and n=4, respectively. Values, mean ± s.d. p values (one-way ANOVA): **p≤0.01 and n.s. not significant.

(E) Cartoon, depicts domain specific binding of IQSEC1 interactors.

(F) PC3 acini expressing ARF5-mNG or ARF6-mNG were stained for Met and LRP1. FIRE LUT images are displayed with magnified images of boxed regions shown in lower panels. White arrowheads indicate localisation in protrusion tips. Scale bars, 5μm (upper) and 10μm (lower).

(G) Schema, colocalization of IQSEC1-ARF interactors in protrusive tips.

(H) Phase images of PC3 acini expressing Scr, *LRP1_1, Met_2, SORL1_1, RICTOR_1* or *SIN1_2* shRNA after 96 hours. Scale bars, 100μm.

(I) Quantitation of images shown in H. Heatmaps show area and compactness measurements as Z-score-normalised values (upper panels). p-values (one-way ANOVA): greyscale values as indicated (lower heatmaps). n=2, 4 replicates/condition, 700-2,400 acini/condition. Cartoon, depicts acini phenotype representative of each condition.

Figure 5. IQSEC1-LRP1 complex regulates Met endocytic trafficking.

(A) Western blot of PC3 cells co-expressing mNG and RFP (Control) or ARF5-mNG and ARF6-RFP (ARF5/6) with either Scr or *IQSEC1* KD4 shRNA. Anti-IQSEC1, phospho-Y1234/1235 Met, Met, phospho-S473 Akt, Akt, and GAPDH (sample control) antibodies were used.

(B) Quantitation of phospho/total Met and phospho/total Akt expression is presented as signal intensity relative to control. n=2 independent experiments. Values, mean ± s.d.

(C) Schema, effect of IQSEC1 on Met trafficking.

(D) PC3 cells expressing Scr or *IQSEC1 KD4* shRNA were incubated with a Met-647 fluorescent antibody at 4°C (Surface) prior to stimulation with HGF for either 10 or 30 minutes (Internalisation). PC3 cells were also treated with chloroquine to allow accumulation of surface-derived Met (black) for 1 hour at 17°C prior to stimulation with HGF for either 10 or 30 minutes (Recycling). Cells were stained with F-actin (green outlines) and Hoechst (nuclei in magenta). Magnified images of boxed regions are inset. Scale bars 20μm.

(E) Intensity of Met antibody in each cell was quantified (Z-score normalised); shown in box-and-whiskers plot: 10–90 percentile; +, mean; dots, outliers; midline, median; boundaries, quartiles. n=2, 4 replicates/condition, minimum 500 cells per condition. p values: (Welsh's t-test).

(F) Intensity of Met antibody in membrane, cytoplasmic and juxtanuclear regions was quantified. Line graphs show relative region intensities compared to the intensity of the whole cell (Z-score normalised). n=2, 4 replicates/condition, minimum 500 cells per condition. p values: (Welsh's t-test).

(G) Schema, sub-cellular re-localisation of active Met upon HGF treatment.

(H) PC3 cells expressing Scr, *IQSEC1 KD4, LRP1* or *SORL1* shRNA were stimulated with HGF for 30 minutes. Cells were stained for phospho-Met (black), F-actin (green outlines) and Hoechst/nuclei (magenta). Magnified images of boxed regions are shown (lower panels). Cartoon, sub-cellular localization of active Met under different conditions.

(I-J) Quantitation of spot intensity (Z-score normalised) is shown for images in H in box-and-whiskers plot: 10–90 percentile; +, mean; dots, outliers; midline, median; boundaries, quartiles. n=2, 4 replicates/condition, minimum 500 cells per condition. p-values (one-way ANOVA).

(K) Schema, regulation of Met internalisation, but not recycling, by IQSEC1 and LRP1.

All p values: n.s. not significant, *p≤0.05, **p≤0.01, ***p≤0.001 and ****p≤0.0001.

Figure 6. IQSEC1-ARF signalling controls phosphoinositide generation in invasive protrusion tips.

(A) Schema, signalling pathways in protrusive tips of PC3 acini.

(B) PC3 acini expressing mNeonGreen tagged PH-PLCδ or PH-Grp1 were fixed after 3 days. PC3 acini were also stained with phospho-S473 Akt antibody. FIRE LUT used to show localisation and intensity of mNeonGreen or pAkt. Magnified images of boxed regions are also shown. White arrowheads, localisation at protrusive tips. Scale bars, 10 μm. Cartoon, spatial PIP production in protrusive tips.

(C) Quantitation of cortical enrichment of $PI(4,5)P_2$ (upper panel) or PIP_3 per cell in the presence or absence of IQSEC1 is shown in box-and-whiskers plot: 10–90 percentile; +, mean; dots, outliers; midline, median; boundaries, quartiles. n=2, 4 replicates/condition, >500 cells/condition. p-values (one-way ANOVA): ****p≤0.0001.

(D) Cartoon, PIPK targeting in presence or absence of IQSEC1.

(E) Western blot of PC3 cells expressing Myr-FLAG-Cre (Control), Myr-FLAG-PIP5Kα, Myr-FLAG-PIP5Kβ or Myr-FLAG-PI3Kβ and either Scr or IQSEC1 shRNA (KD4). Anti-IQSEC1, phospho-S473 Akt, total Akt and GAPDH antibodies were used. GAPDH is shown for IQSEC1 blot.

(F) Western blot of PC3 cells expressing Myr-FLAG-Cre (Control) or Myr-Akt1 and either Scr or *IQSEC1* KD4 shRNA using anti-IQSEC1, phospho-S473 Akt, total Akt and GAPDH antibodies. GAPDH is shown for IQSEC1 blot.

(G) Phase images of PC3 acini described in E are shown. Scr acini were also treated with NAV-2729 (IQSEC1 inhibitor). Scale bars, 100µm.

(H) Quantitation of images shown in G. Heatmaps show area and compactness measurements as Z-score-normalised values (upper panels). p-values (one-way ANOVA): greyscale values as indicated (lower heatmaps). n=3 with 4 replicates per condition. Between 1,693 and 2,435 acini quantified per condition. Cartoon, acini phenotype representative of each condition.

(I) Phase images of PC3 acini described in F after 96 hours. Scr acini were also treated with IQSEC1-inhibiting compound NAV-2729. Scale bars, 100µm.

(J) Quantitation of images shown in I. n=2 with 4 replicates/condition, 1,287-2,363 acini/condition. Cartoon, acini phenotype representative of each condition.

(K) Schema, summarizes the relationship between location and level of cortical PIP_3 and 2D and 3D PC3 phenotype.

Figure 7. IQSEC1 regulates growth and invasion *in vivo* and IQSEC1-ARF signalling is associated with poor patient outcome.

(A) Schema, intraprostatic transplantation of PC3 cells expressing either Scr (control, 12 mice) or *IQSEC1* KD4 shRNA (10 mice) into CD1-nude male mice. Tumour growth was determined after 8 weeks using ultrasound and the incidence and location of macromets counted.

(B) Bar graph shows prostate tumour incidence (% mice). p-values (Chi-squared).

(C) Ultrasound images show area and volume of representative prostate tumours in mice injected with PC3 cells expressing either Scr or IQSEC1 KD4.

(D-E) Area **(D)** and volume **(E)** of each prostate tumour detectable by ultrasound was measured. p-values (Mann-Whitney). Multiple prostate tumours were detected in some mice.

(F-G) Macrometastasis incidence was counted and is presented as % mice. **(F)** and count per mouse **(G).** p-values (Chi-squared and Mann-Whitney respectively).

(H) Heatmap shows the frequency at which metastasis occurred at locations with different proximity to the prostate. Cartoon, summarizes the locations metastasis was observed.

(I-L) Quantitation of *ARF5* and *ARF6* expression levels in either 52 normal or 487 tumour samples **(I-J)** or in 29 normal, 131 primary or 19 metastatic tumours **(K-L)** (TCGA). Box-and-whiskers plot: 10–90 percentile; +, mean; dots, outliers; midline,

median; boundaries, quartiles. p-values (one-way ANOVA). All p values: n.s. not significant, *p≤0.05, **p≤0.01 and ****p≤0.0001.

(M) *IQSEC1, ARF5* and *ARF6* gene expression from 79 primary tumours (GSE25136) was evaluated for outcome prediction from (recurrence-free) survival data. Patient samples were clustered into 4 groups (kmeans) based on normalized gene expression. Inset heatmap shows clustering of expression values. p-values (Logrank) are annotated in plots.

(N) Schematic depicting the signalling mechanisms involved in IQSEC1 dependent model of prostate cancer growth and invasion.

Supplementary Figure 1. IQSEC1 is a regulator of cell elongation and collective invasion.

(A) Graph generated using RNAseq data from CCLE comparing *IQSEC2* gene copy number and mRNA expression levels in multiple breast and prostate cancer and non-transformed cell lines.

(B-C) Quantitation of *IQSEC2* expression levels in either 52 normal or 487 prostate tumour samples (TCGA) **(B)** or in 29 normal, 131 primary or 19 metastatic prostate tumour tissues (GSE21034) **(C)**. Box-and-whiskers plot: 10–90 percentile; +, mean; dots, outliers; midline, median; boundaries, quartiles. p-values (one-way ANOVA): n.s. not significant, and ****p≤0.0001.

(D) *IQSEC2* gene expression from 487 primary prostate tumours (TCGA) was evaluated for outcome prediction from (recurrence-free) survival data. Patient samples were clustered into quartiles based on normalized gene expression. Highest expression, red, lowest expression, blue. Inset Heatmap shows clustering of expression values. p-values (Logrank) are annotated in plots.

(E) Western blot of PC3 cells stably expressing Scrambled (Scr) or *IQSEC1* (KD1, KD4) shRNAs using anti-IQSEC1 and GAPDH (loading control for IQSEC1 blot) antibodies. Arrowheads indicate reduction of three major bands. IQSEC1 intensity for all bands combined normalised to Scr control is shown. n=3 independent experiments. Values are mean ± s.d.

(F) PC3 cells expressing Scr or *IQSEC1* KD shRNA were imaged every hour for 3.5 days. Cell confluence was measured and normalised to control. Values are mean ± s.d. p-values (Students t-test) are annotated in plot.

(G) Schematic of phenotypic analysis of PC3 cells in 2D. Machine learning applied to confocal images to classify and quantify cells into 3 categories based on shape: spindle, spread, round.

(H) PC3 cells expressing Scr or *IQSEC1* KD4 shRNA were stained with whole cell stain (WCS) (red) and Hoechst/nuclei (blue) (left panels). Cells were classified into spindle, spread and round phenotypes shown in green, red and blue respectively (right panels). Scale bar, 100µm.

(I-J) Proportion of PC3 cells with each phenotype **(I)** or classified into round, spindle or spread **(J)** is shown. Heatmap indicates log2 fold change of each phenotype over Scr (upper heatmap). p-values (one-way ANOVA): greyscale values as indicated (lower heatmap). n=4 independent experiments, 10 replicates per condition, minimum 118,000 cells imaged/condition.

(K-L) Schema, PC3 cells plated for 24 hours before the resultant monolayers were **(K)** wounded or **(L)** wounded and overlaid with 25% ECM for 1 hour prior to imaging using 10x objective. Phase contrast images are shown where the yellow dashed lines indicate initial scratch wound and red pseudo colour shows wound after 24 hours. Magnified images of boxed areas are shown for different time points. Relative wound density (RWD) was calculated at each time point and graphed (lower left panels). RWD at the time point where the Scr controls are 50% closed ($t=Max_{1/2}$) is also shown (lower right panels). Samples were normalised to the average of all Scr controls across experiments. n=3, 3 replicates/experiment in K and 4 in L. Values, mean ± s.d. p-values (Student's t-test): *$p \leq 0.05$, **$p \leq 0.01$ and ****$p \leq 0.0001$.

(M) Schema, depicts invasive ability of PC3 in ECM in the presence or absence of IQSEC1.

(N) Schema, summarizes the effect IQSEC1 depletion has on 2D growth, shape and migration and on 3D invasion.

Supplementary Figure 2. IQSEC1 v2 induces spindle shape and protrusive invasion.

(A) Schema, outlines generated by CellProfiler were colour- coded at each time point and overlaid in 12 hour blocks using Fiji. Scale bars, 20µm.

(B) Phase contrast images are shown for PC3 acini expressing Scr or *IQSEC1* KD4 shRNA. Acini outlines, yellow. Magnified images of boxed regions are shown at different time points. Scale bars, 100µm.

(C) Quantitation of images shown in B. CellProfiler was used to measure invasion parameters i.e. area and compactness, over 4 days, in 12 hour blocks. Quantitation shown as Z-score-normalised values (upper heatmap). p-values (one-way ANOVA): greyscale values as indicated (lower heatmap). n=4, 4 replicates/condition, 1,555-2,035 acini/condition.

(D) PC3 cells expressing GFP or GFP-IQSEC1 v1-4 and either Scr or *IQSEC1* KD4 shRNA classified into spindle, spread and round phenotypes shown in green, red and blue respectively (right panels). Scale bars, 100μm. Quantitation is shown in heatmaps as log2 fold change of each phenotype over control (top row in left heatmap). p-values (one-way ANOVA): greyscale values as indicated (right heatmap). n=2, 4 replicates/condition, 1,431-5,587 cells quantified/condition.

(E) Cells were also analysed for nuclear, cytoplasmic and membrane localisation of GFP using Harmony High-Content Imaging and Analysis Software. Quantitation is shown in heatmaps. n=2, 4 replicates per condition.

(F) Schemes, IQSEC1 chimeras generated by swapping N- and C- terminal domains from IQSEC1 variants v1-v4. Colour coding as follows: v1 = blue, v2 = pink and v4 = green. Chimeras with alternate N-termini, C-termini or are GEF dead are labelled (a), (b) or (c) respectively.

(G) PC3 cells expressing GFP, GFP-IQSEC1 v2 or GFP-IQSEC1 chimeras and either Scr or *IQSEC1* KD4 shRNA were classified into spindle, spread and round phenotypes. n=2, 4 replicates/condition, 10,000-35,000 cells/condition.

(H) Cells from G were also analysed for nuclear, cytoplasmic and membrane localisation and quantitation is shown in heatmaps. n=2, 4 replicates/condition.

(I) PC3 acini expressing GFP, GFP-IQSEC1 v2 or GFP-IQSEC1 chimeras were fixed after 3 days and FIRE LUT used to show localisation and intensity of GFP. Magnified images of boxed regions are also shown in lower panels. Scale bars, 10μm.

(J) Phase images from PC3 acini described in I are shown after 96 hours. GFP-positive acini are outlined in yellow. Scale bars, 100μm.

(K) Quantitation of images shown in J. n=2, 4 replicates/condition, 550-1,662 cysts/condition. Cartoon, depicts acini phenotype representative of each condition.

(L) Schema, depicts the role of IQSEC1 v1 and v2 termini on localization and invasion.

Supplementary Figure 3. ARF5 and ARF6 co-operate to regulate both growth and invasion.

(A) Quantitation of shape classification of PC3 cells expressing Scr, *ARF5, ARF6* or *AR5/6* shRNA is shown. Heatmaps show log2 fold change of each phenotype over control (left heatmaps). p-values (one-way ANOVA): greyscale values as indicated (right heatmaps). n=2, 4 replicates. Minimum of 4,000 cells/condition analysed in total.

(B) Schema, comparison of activation of WT ARF GTP and fast-cycling ARF mutants.

(C) Western blot of PC3 cells expressing mNG, ARF5-mNG, ARF5-mNG fast cycling (TA), ARF6-mNG or ARF6-mNG fast cycling (TN) using anti-ARF5, ARF6 and GAPDH (shown for ARF5 blot) antibodies.

(D) Quantitation of shape classification of PC3 cells described in C is shown. n=2, 4 replicates.

(E) Quantitation of PC3 acini described in C. Heatmaps show area and compactness measurements as Z-score-normalised values (upper heatmap). p-values (one-way ANOVA): greyscale values as indicated (lower heatmap). n=2 with 4 replicates per condition. Minimum of 900 acini/condition analysed in total. Cartoon, depicts acini phenotype representative of each condition.

(F) Quantitation of shape classification of PC3 cells expressing mNG, ARF5-mNG and ARF6-RFP or ARF5-mNG TA and ARF6-RFP TN is shown. n=3, 3 replicates.

(G) Quantitation of PC3 acini. n=2, 4 replicates. Cartoon, depicts acini phenotype representative of each condition.

(H) Quantitation of shape classification of PC3 cells expressing control or ARF5/ARF6 and Scr or *IQSEC1* KD4 shRNA. n=2, 4 replicates.

(I) PC3 cells expressing Scr or *IQSEC1* shRNA were serum starved overnight and HGF was then added for 30 minutes. GGA3 pulldown was carried out and western blot analysis performed using anti-IQSEC1, ARF5, ARF6, and GAPDH (shown for ARF6 blot) antibodies. Quantitation of ARF5 and ARF6 GTP loading normalised to control is shown (right panels). n=3 independent experiments. Values, mean ± s.d. p-values (one-way ANOVA): no significance.

(J) Schema**,** modulation of ARF activity using SecinH3, NAV-2729 or QS11.

(K) *In vitro* fluorescent polarisation assay was carried out to study exchange of fluorescent nucleotides (MANT) on ARF5. IQSEC1 v2 SEC7-PH WT and GEF dead

mutant IQSEC1 v2 SEC7-PH GEF* were used to test the role of IQSEC1 in activation of ARF5. ARFs, nucleotides, GEFs and inhibitors were added at time points indicated. Changes in polarisation over time are shown.

(L) Western blot of PC3 cells treated for 24 hours with NAV-2729, SecinH3 or QS11 using anti-IQSEC1, ARF5, ARF6 and GAPDH (shown for IQSEC1) antibodies.

(M) Representative phase contrast images of PC3 acini treated with NAV-2729, SecinH3 or QS11 after 96 hours. Scale bars, 100µm.

(N) Quantitation of PC3 acini shown in M. n=1, 4 replicates.

(O) Cartoon, depicts representative acini phenotype upon treatment with inhibitors.

Supplementary Figure 4. IQSEC1 interacts with multiple transmembrane proteins.

(A) GFP-trap immunoprecipitation was performed on PC3 cells expressing GFP, GFP-IQSEC1 v2 or v4. Western blot analysis was then carried out using anti-IQSEC1, LRP1, Met, SORL1, RICTOR, Sin1, ARFGAP1, 14-3-3ζ/Δ, PPC6, GFP and GAPDH (shown for GFP blot) antibodies.

(B) Western blot of PC3 subclones using anti-IQSEC1, ARF5, ARF6, ARFGAP1, LRP1, phospho-Y1234/1235 Met, Met, SORL1, RICTOR and GAPDH (shown for IQSEC1 blot) antibodies.

(C) Western blot of Epi and EMT14 PC3 subclones using anti-IQSEC1, ARF5, ARF6, ARFGAP1, LRP1, phospho-Y1234/1235 Met, Met, SORL1, RICTOR and GAPDH (shown for IQSEC1 blot) antibodies.

(D) Met immunoprecipitation was carried out on PC3 cells expressing Scr or *IQSEC1* KD4 shRNA. Western blot was then performed on lysates (upper panels) and IPs (lower panels) using anti-LRP1, Met, IQSEC1 and GAPDH (shown for IQSEC1 blot) antibodies. Quantitation of LRP1/Met interaction normalised to Scr is shown. Values, mean ± s.d. n=3 independent experiments. p values (one-way ANOVA): n.s. not significant.

(E-F) Western blot analysis of PC3 cells expressing Scr or **(E)** *LRP1* and **(F)** *Met* shRNA. GAPDH is shown for Akt blots.

(G) Quantitation of shape classification of PC3 cells expressing shRNAs for IQSEC1 binding partners as log2 fold change of each phenotype over control (left heatmap). p-values (one-way ANOVA): greyscale values as indicated (right heatmap). n=2, 4 replicates per condition, minimum 14,000 cells imaged/condition.

(H) Quantitation of PC3 acini expressing GFP or LRP1-GFP. Heatmaps for area and compactness measurements shown as Z-score-normalised values (upper heatmap). p-values (one-way ANOVA): greyscale values as indicated (lower heatmap). n=3, 3 replicates, minimum 150 acini/condition.

(I) Western blot of PC3 cells expressing *SORL1* shRNA. GAPDH is shown for Akt blots.

(J) Representative phase contrast images of PC3 acini expressing Scr (also shown in Figure 4H), *SORL1*_2 and *RICTOR_2* shRNA taken after 96 hours. Scale bars, 100μm.

(K) Quantitation of PC3 acini shown in J. n=2, 4 replicates, minimum 700 acini/condition.

(L-N) Western blots of PC3 cells expressing **(L)** *RICTOR* or **(M)** *SIN1* or **(N)** *ARFGAP1* shRNA. GAPDH is shown for Akt blots.

(O) Representative phase contrast images of PC3 acini expressing Scr, *ARFGAP1_1* and *ARFGAP1_2* shRNA taken after 96 hours. Scale bars, 100μm.

(P) Quantitation of PC3 acini shown in O. n=2, 4 replicates, minimum 1,100 acini/condition.

(Q) Cartoon, depicts representative acini phenotype upon depletion of ARFGAP1 and ARF GTPase cycle.

Supplementary Figure 5. HGF stimulation is abrogated by IQSEC1 depletion.

(A) Western blot of PC3 cells expressing Scr or *IQSEC1* KD4 shRNA stimulated with HGF for 30 minutes using anti-IQSEC1, phospho-Y1234/1235 Met, Met, phospho-S473 Akt, Akt, ARF5, ARF6 and GAPDH (shown for Akt blot) antibodies.

(B) Quantitation of phospho/total Met and phospho/total Akt expression is presented as signal intensity relative to control. Values, mean ± s.d. n=3 independent experiments.

(C) Phase contrast images of PC3 acini expressing Scr or *IQSEC1* KD4 shRNA stimulated with HGF for 96 hours. Scale bars, 100μm. Cartoon, depicts acini phenotype representative of each condition.

(D) Quantitation of PC3 acini shown in C. Heatmaps show area and compactness measurements as Z-score-normalised values (upper panels). p-values (one-way ANOVA): greyscale values as indicated (lower heatmap). n=3, 4 replicates/condition, 1,400-4,025 acini/condition.

(E) Western blots of PC3 cells expressing Scr or *IQSEC1* KD4 shRNA treated with cycloheximide (CHX) for various times using anti-IQSEC1, Met and GAPDH (shown for Met blot) antibodies. Quantitation of Met expression levels normalised to time 0 is shown. Values, mean ± s.e. n=3. p-values (one-way ANOVA): *p≤0.05, ***p≤0.001 and ****p≤0.0001.

Supplementary Figure 6. IQSEC1-ARF controls cortical PI(4,5)P_2 generation, which is required for production of PIP_3.

(A) PC3 cells expressing mNeonGreen tagged PH-PLCδ (PIP_2) or PH-Grp1 (PIP_3) and either Scr or *IQSEC1* shRNA KD4 were fixed after 2 days. FIRE LUT is used to show localisation and intensity of GFP in magnified images of boxed regions. White arrowhead indicates localisation at protrusive tip. Scale bars, 20μm.

(B-C) Quantitation of **(B)** PI(4,5)P_2 or **(C)** PIP_3 cortical enrichment in spindle, spread and round cells expressing either Scr or IQSEC1 KD4 shRNA is shown in box-and-whiskers plot: 10–90 percentile; +, mean; dots, outliers; midline, median; boundaries, quartiles. n=3, 4 replicates/condition. 1330/1049 and 2222/1182 cells analysed for Src/*IQSEC1* KD4 shRNA respectively in B and C. p-values (one-way ANOVA).

(D) Cartoon, summary of cortical PI(4,5)P_2 and PIP_3 localization in different cell shapes.

(E) Western blot of PC3 cells treated with LY294002 (pan PI3K), AZD8835 (PI3Kα), AZD8186 (PI3Kβ), AS605240 (PI3Kγ), Cal-101 (PI3Kδ) and AktII (Akt) inhibitors for 24 hours. Anti-phospho-S473 Akt, Akt and GAPDH antibodies were used.

(F) Phase contrast images of PC3 acini described in E. Scale bars, 100μm.

(G) Cartoon, depicts acini phenotype representative of each condition.

(H) Quantitation of PC3 acini shown in F. Heatmaps show area and compactness measurements as Z-score-normalised values (upper heatmaps). p-values (one-way ANOVA): greyscale values as indicated (lower heatmaps). n=2, 4 replicates, minimum of 350 acini/condition.

(I) Western blot of PC3 cells expressing Scr, PIP5K1α or PIP5K1β shRNA using anti-PIP5K, IQSEC1, phospho-S473 Akt, Akt and GAPDH (shown for Akt blots) antibodies.

(J) Phase contrast images of PC3 acini expressing Scr, PIP5K1α or PIP5K1β shRNA at 96 hours. Scale bars, 100μm.

(K) Quantitation of PC3 acini shown in J. n=2, 4 replicates, minimum of 1,348 acini/condition. Cartoon, depicts acini phenotype representative of each condition.
(L) PC3 cells expressing Scr or *IQSEC1* KD4 shRNA were stained for pS473 Akt (black) and Hoechst /nuclei (magenta). Magnified images of boxed regions are shown in lower panels. Blue arrowheads indicate localisation of active Akt. Scale bars, 10µm.
(M-N) Quantitation of pAkt **(M)** intensity or **(N)** area in spots in the juxtanuclear, cytoplasm and periphery of PC3 cells expressing either Scr or IQSEC1 KD4 shRNA. Box-and-whiskers plots: 10–90 percentile; +, mean; dots, outliers; midline, median; boundaries, quartiles. n=2, 4 replicates/condition. p values (Mann Whitney).
(O) Cartoon, depicting phospho-Akt intensity, in the presence or absence of IQSEC1, at different subcellular locations.
All p-values: n.s. not significant, *p≤0.05, **p≤0.01, ***p≤0.001 and ****p≤0.0001.

Supplementary Figure 7. IQSEC1 regulates growth and invasion in multiple prostate cancer cell lines.
(A) Heatmap shows mRNA expression levels, mined from CCLE, of the Met-PI3K-Akt pathway across different prostate cancer cell lines.
(B) Western blot of prostate cancer cell lines using anti-IQSEC1, phospho-Y1234/1234 Met, total Met, LRP1, ARF5, ARF6 and GAPDH antibodies. GAPDH is shown for ARF6 blot.
(C) Schema, effect of NAV-2729 on ARF GTPase cycle.
(D) Phase images of acini (+ and – HGF) at different time points are shown. Acini were also treated with NAV-2729 for 96 hours. Scale bars, 100µm.
(E) Schema, summarizes the effect of each treatment described in D on acini growth and invasion.
(F-I) Quantitation of 22Rv1 **(F)**, LNCaP **(G)**, DU145 **(H)** and DU145 + HGF **(I)** acini formation in the absence or presence of NAV-2729. 22Rv1 and DU145 acini were also expressing LRP1-GFP and IQSEC1-GFP v2 respectively. Heatmaps show area and compactness measurements as Z-score-normalised values (upper panels). p-values (one-way ANOVA): greyscale values as indicated (lower heatmap). n=2, replicates/condition, 400-1600 acini/condition.

References

1. Halaoui, R. & McCaffrey, L. Rewiring cell polarity signaling in cancer. *Oncogene* **34**, 939-950 (2015).
2. Pampaloni, F., Reynaud, E.G. & Stelzer, E.H. The third dimension bridges the gap between cell culture and live tissue. *Nature reviews. Molecular cell biology* **8**, 839-845 (2007).
3. Bryant, D.M. & Mostov, K.E. From cells to organs: building polarized tissue. *Nature reviews. Molecular cell biology* **9**, 887-901 (2008).
4. Zajac, O. *et al.* Tumour spheres with inverted polarity drive the formation of peritoneal metastases in patients with hypermethylated colorectal carcinomas. *Nature cell biology* **20**, 296-306 (2018).
5. Bryant, D.M. *et al.* A molecular switch for the orientation of epithelial cell polarization. *Developmental cell* **31**, 171-187 (2014).
6. Shamir, E.R. & Ewald, A.J. Three-dimensional organotypic culture: experimental models of mammalian biology and disease. *Nature reviews. Molecular cell biology* **15**, 647-664 (2014).
7. Parachoniak, C.A. & Park, M. Dynamics of receptor trafficking in tumorigenicity. *Trends in cell biology* **22**, 231-240 (2012).
8. Joffre, C. *et al.* A direct role for Met endocytosis in tumorigenesis. *Nature cell biology* **13**, 827-837 (2011).

9. Menard, L., Parker, P.J. & Kermorgant, S. Receptor tyrosine kinase c-Met controls the cytoskeleton from different endosomes via different pathways. *Nature communications* **5**, 3907 (2014).
10. Parachoniak, C.A., Luo, Y., Abella, J.V., Keen, J.H. & Park, M. GGA3 functions as a switch to promote Met receptor recycling, essential for sustained ERK and cell migration. *Developmental cell* **20**, 751-763 (2011).
11. Humphreys, D., Davidson, A.C., Hume, P.J., Makin, L.E. & Koronakis, V. Arf6 coordinates actin assembly through the WAVE complex, a mechanism usurped by Salmonella to invade host cells. *Proceedings of the National Academy of Sciences of the United States of America* **110**, 16880-16885 (2013).
12. Montagnac, G. *et al.* ARF6 Interacts with JIP4 to control a motor switch mechanism regulating endosome traffic in cytokinesis. *Current biology : CB* **19**, 184-195 (2009).
13. Moravec, R., Conger, K.K., D'Souza, R., Allison, A.B. & Casanova, J.E. BRAG2/GEP100/IQSec1 interacts with clathrin and regulates alpha5beta1 integrin endocytosis through activation of ADP ribosylation factor 5 (Arf5). *The Journal of biological chemistry* **287**, 31138-31147 (2012).
14. Rainero, E. *et al.* Ligand-Occupied Integrin Internalization Links Nutrient Signaling to Invasive Migration. *Cell reports* **10**, 398-413 (2015).
15. Santy, L.C., Ravichandran, K.S. & Casanova, J.E. The DOCK180/Elmo complex couples ARNO-mediated Arf6 activation to the downstream activation of Rac1. *Current biology : CB* **15**, 1749-1754 (2005).
16. Stamnes, M.A. & Rothman, J.E. The binding of AP-1 clathrin adaptor particles to Golgi membranes requires ADP-ribosylation factor, a small GTP-binding protein. *Cell* **73**, 999-1005 (1993).
17. Donaldson, J.G. & Jackson, C.L. ARF family G proteins and their regulators: roles in membrane transport, development and disease. *Nature reviews. Molecular cell biology* **12**, 362-375 (2011).
18. Hashimoto, A. *et al.* GEP100-Arf6-AMAP1-cortactin pathway frequently used in cancer invasion is activated by VEGFR2 to promote angiogenesis. *PloS one* **6**, e23359 (2011).
19. Hashimoto, S. *et al.* Lysophosphatidic acid activates Arf6 to promote the mesenchymal malignancy of renal cancer. *Nature communications* **7**, 10656 (2016).
20. Kinoshita, R. *et al.* Co-overexpression of GEP100 and AMAP1 proteins correlates with rapid local recurrence after breast conservative therapy. *PloS one* **8**, e76791 (2013).
21. Morishige, M. *et al.* GEP100 links epidermal growth factor receptor signalling to Arf6 activation to induce breast cancer invasion. *Nature cell biology* **10**, 85-92 (2008).
22. Hashimoto, S. *et al.* Targeting AMAP1 and cortactin binding bearing an atypical src homology 3/proline interface for prevention of breast cancer invasion and metastasis. *Proceedings of the National Academy of Sciences of the United States of America* **103**, 7036-7041 (2006).
23. Grossmann, A.H. *et al.* The small GTPase ARF6 stimulates beta-catenin transcriptional activity during WNT5A-mediated melanoma invasion and metastasis. *Science signaling* **6**, ra14 (2013).
24. Marchesin, V. *et al.* ARF6-JIP3/4 regulate endosomal tubules for MT1-MMP exocytosis in cancer invasion. *The Journal of cell biology* **211**, 339-358 (2015).

25. Marchesin, V., Montagnac, G. & Chavrier, P. ARF6 promotes the formation of Rac1 and WAVE-dependent ventral F-actin rosettes in breast cancer cells in response to epidermal growth factor. *PloS one* **10**, e0121747 (2015).
26. Muralidharan-Chari, V. *et al.* ADP-ribosylation factor 6 regulates tumorigenic and invasive properties in vivo. *Cancer research* **69**, 2201-2209 (2009).
27. Zhang, Q. *et al.* Small-molecule synergist of the Wnt/beta-catenin signaling pathway. *Proceedings of the National Academy of Sciences of the United States of America* **104**, 7444-7448 (2007).
28. Singh, M.K. *et al.* Structure-activity relationship studies of QS11, a small molecule Wnt synergistic agonist. *Bioorganic & medicinal chemistry letters* **25**, 4838-4842 (2015).
29. Yoo, J.H. *et al.* ARF6 Is an Actionable Node that Orchestrates Oncogenic GNAQ Signaling in Uveal Melanoma. *Cancer cell* **29**, 889-904 (2016).
30. Bello, D., Webber, M.M., Kleinman, H.K., Wartinger, D.D. & Rhim, J.S. Androgen responsive adult human prostatic epithelial cell lines immortalized by human papillomavirus 18. *Carcinogenesis* **18**, 1215-1223 (1997).
31. Kaighn, M.E., Narayan, K.S., Ohnuki, Y., Lechner, J.F. & Jones, L.W. Establishment and characterization of a human prostatic carcinoma cell line (PC-3). *Investigative urology* **17**, 16-23 (1979).
32. Someya, A. *et al.* ARF-GEP(100), a guanine nucleotide-exchange protein for ADP-ribosylation factor 6. *Proceedings of the National Academy of Sciences of the United States of America* **98**, 2413-2418 (2001).
33. Dunphy, J.L., Ye, K. & Casanova, J.E. Nuclear functions of the Arf guanine nucleotide exchange factor BRAG2. *Traffic* **8**, 661-672 (2007).
34. Manavski, Y. *et al.* Brag2 differentially regulates beta1- and beta3-integrin-dependent adhesion in endothelial cells and is involved in developmental and pathological angiogenesis. *Basic research in cardiology* **109**, 404 (2014).
35. Santy, L.C. Characterization of a fast cycling ADP-ribosylation factor 6 mutant. *The Journal of biological chemistry* **277**, 40185-40188 (2002).
36. Beemiller, P., Hoppe, A.D. & Swanson, J.A. A phosphatidylinositol-3-kinase-dependent signal transition regulates ARF1 and ARF6 during Fcgamma receptor-mediated phagocytosis. *PLoS biology* **4**, e162 (2006).
37. Hafner, M. *et al.* Inhibition of cytohesins by SecinH3 leads to hepatic insulin resistance. *Nature* **444**, 941-944 (2006).
38. Benabdi, S. *et al.* Family-wide Analysis of the Inhibition of Arf Guanine Nucleotide Exchange Factors with Small Molecules: Evidence of Unique Inhibitory Profiles. *Biochemistry* **56**, 5125-5133 (2017).
39. Lu, Z.X. *et al.* Transcriptome-wide landscape of pre-mRNA alternative splicing associated with metastatic colonization. *Molecular cancer research : MCR* **13**, 305-318 (2015).
40. Roca, H. *et al.* Transcription factors OVOL1 and OVOL2 induce the mesenchymal to epithelial transition in human cancer. *PloS one* **8**, e76773 (2013).
41. Lillis, A.P., Mikhailenko, I. & Strickland, D.K. Beyond endocytosis: LRP function in cell migration, proliferation and vascular permeability. *Journal of thrombosis and haemostasis : JTH* **3**, 1884-1893 (2005).

42. Herz, J. *et al.* Surface location and high affinity for calcium of a 500-kd liver membrane protein closely related to the LDL-receptor suggest a physiological role as lipoprotein receptor. *The EMBO journal* **7**, 4119-4127 (1988).
43. Li, H. *et al.* Targeting of mTORC2 prevents cell migration and promotes apoptosis in breast cancer. *Breast cancer research and treatment* **134**, 1057-1066 (2012).
44. Zhang, F. *et al.* mTOR complex component Rictor interacts with PKCzeta and regulates cancer cell metastasis. *Cancer research* **70**, 9360-9370 (2010).
45. Liu, P. *et al.* Sin1 phosphorylation impairs mTORC2 complex integrity and inhibits downstream Akt signalling to suppress tumorigenesis. *Nature cell biology* **15**, 1340-1350 (2013).
46. Jian, X. *et al.* Autoinhibition of Arf GTPase-activating protein activity by the BAR domain in ASAP1. *The Journal of biological chemistry* **284**, 1652-1663 (2009).
47. Lewis, S.M., Poon, P.P., Singer, R.A., Johnston, G.C. & Spang, A. The ArfGAP Glo3 is required for the generation of COPI vesicles. *Molecular biology of the cell* **15**, 4064-4072 (2004).
48. Zhang, C.J., Cavenagh, M.M. & Kahn, R.A. A family of Arf effectors defined as suppressors of the loss of Arf function in the yeast Saccharomyces cerevisiae. *The Journal of biological chemistry* **273**, 19792-19796 (1998).
49. Theret, L. *et al.* Identification of LRP-1 as an endocytosis and recycling receptor for beta1-integrin in thyroid cancer cells. *Oncotarget* **8**, 78614-78632 (2017).
50. Kang, H.S. *et al.* LRP1-dependent pepsin clearance induced by 2'-hydroxycinnamaldehyde attenuates breast cancer cell invasion. *The international journal of biochemistry & cell biology* **53**, 15-23 (2014).
51. Stephens, L. *et al.* Protein kinase B kinases that mediate phosphatidylinositol 3,4,5-trisphosphate-dependent activation of protein kinase B. *Science* **279**, 710-714 (1998).
52. Sarbassov, D.D., Guertin, D.A., Ali, S.M. & Sabatini, D.M. Phosphorylation and regulation of Akt/PKB by the rictor-mTOR complex. *Science* **307**, 1098-1101 (2005).
53. Brown, H.A., Gutowski, S., Moomaw, C.R., Slaughter, C. & Sternweis, P.C. ADP-ribosylation factor, a small GTP-dependent regulatory protein, stimulates phospholipase D activity. *Cell* **75**, 1137-1144 (1993).
54. Cockcroft, S. *et al.* Phospholipase D: a downstream effector of ARF in granulocytes. *Science* **263**, 523-526 (1994).
55. Honda, A. *et al.* Phosphatidylinositol 4-phosphate 5-kinase alpha is a downstream effector of the small G protein ARF6 in membrane ruffle formation. *Cell* **99**, 521-532 (1999).
56. Yoo, J.H. *et al.* The small GTPase ARF6 activates PI3K in melanoma to induce a pro-metastatic state. *Cancer research* (2019).
57. Tsai, M.T. *et al.* Regulation of HGF-induced hepatocyte proliferation by the small GTPase Arf6 through the PIP2-producing enzyme PIP5K1A. *Scientific reports* **7**, 9438 (2017).
58. Luo, L. *et al.* TLR Crosstalk Activates LRP1 to Recruit Rab8a and PI3Kgamma for Suppression of Inflammatory Responses. *Cell reports* **24**, 3033-3044 (2018).
59. Volpicelli-Daley, L.A., Li, Y., Zhang, C.J. & Kahn, R.A. Isoform-selective effects of the depletion of ADP-ribosylation factors 1-5 on membrane traffic. *Molecular biology of the cell* **16**, 4495-4508 (2005).

60. Ceccarelli, D.F. *et al.* Non-canonical interaction of phosphoinositides with pleckstrin homology domains of Tiam1 and ArhGAP9. *The Journal of biological chemistry* **282**, 13864-13874 (2007).
61. Zhu, W. *et al.* Small GTPase ARF6 controls VEGFR2 trafficking and signaling in diabetic retinopathy. *The Journal of clinical investigation* **127**, 4569-4582 (2017).
62. Ratcliffe, C.D.H. *et al.* HGF-induced migration depends on the PI(3,4,5)P3-binding microexon-spliced variant of the Arf6 exchange factor cytohesin-1. *The Journal of cell biology* **218**, 285-298 (2019).
63. Klarlund, J.K., Tsiaras, W., Holik, J.J., Chawla, A. & Czech, M.P. Distinct polyphosphoinositide binding selectivities for pleckstrin homology domains of GRP1-like proteins based on diglycine versus triglycine motifs. *The Journal of biological chemistry* **275**, 32816-32821 (2000).
64. Ogasawara, M. *et al.* Similarities in function and gene structure of cytohesin-4 and cytohesin-1, guanine nucleotide-exchange proteins for ADP-ribosylation factors. *The Journal of biological chemistry* **275**, 3221-3230 (2000).
65. Roman-Fernandez, A. *et al.* The phospholipid PI(3,4)P2 is an apical identity determinant. *Nature communications* **9**, 5041 (2018).
66. Somers, K.D. *et al.* Orthotopic treatment model of prostate cancer and metastasis in the immunocompetent mouse: efficacy of flt3 ligand immunotherapy. *International journal of cancer* **107**, 773-780 (2003).
67. Hubner, N.C. *et al.* Quantitative proteomics combined with BAC TransgeneOmics reveals in vivo protein interactions. *The Journal of cell biology* **189**, 739-754 (2010).
68. Cox, J. & Mann, M. MaxQuant enables high peptide identification rates, individualized p.p.b.-range mass accuracies and proteome-wide protein quantification. *Nature biotechnology* **26**, 1367-1372 (2008).
69. Cox, J. *et al.* Andromeda: a peptide search engine integrated into the MaxQuant environment. *Journal of proteome research* **10**, 1794-1805 (2011).
70. UniProt, C. The Universal Protein Resource (UniProt) in 2010. *Nucleic acids research* **38**, D142-148 (2010).
71. Cox, J. *et al.* Accurate proteome-wide label-free quantification by delayed normalization and maximal peptide ratio extraction, termed MaxLFQ. *Molecular & cellular proteomics : MCP* **13**, 2513-2526 (2014).
72. Perez-Riverol, Y. *et al.* The PRIDE database and related tools and resources in 2019: improving support for quantification data. *Nucleic acids research* **47**, D442-D450 (2019).

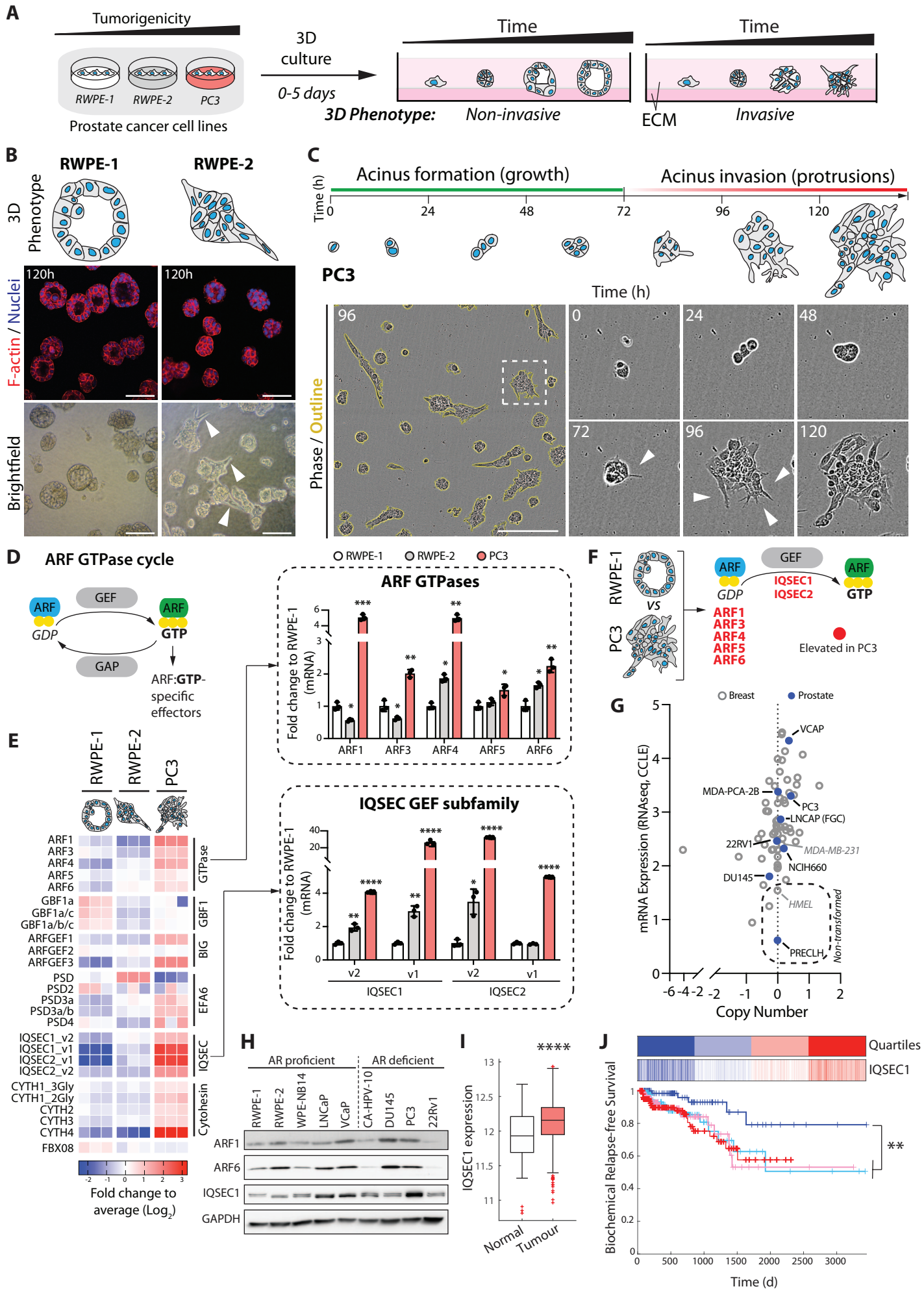
A
Tumorigenicity
RWPE-1
RWPE-2
PC3
Prostate cancer cell lines
3D culture
0-5 days
Time
3D Phenotype:
Non-invasive
ECM
Invasive
B
RWPE-1
RWPE-2
3D Phenotype
F-actin / Nuclei
Brightfield
120h
C
Acinus formation (growth)
Acinus invasion (protrusions)
Time (h)
PC3
Phase / Outline
D
ARF GTPase cycle
GEF
GAP
ARF
GDP
GTP
ARF:GTP-specific effectors
RWPE-1
RWPE-2
PC3
ARF GTPases
Fold change to RWPE-1 (mRNA)
ARF1
ARF3
ARF4
ARF5
ARF6
IQSEC GEF subfamily
IQSEC1
IQSEC2
v2
v1
E
GTPase
GBF1
BIG
EFA6
IQSEC
Cytohesin
Fold change to average (Log2)
F
RWPE-1
PC3
vs
IQSEC1
IQSEC2
Elevated in PC3
G
Breast
Prostate
VCAP
MDA-PCA-2B
PC3
LNCAP (FGC)
22RV1
MDA-MB-231
NCIH660
DU145
HMEL
PRECLH
Non-transformed
mRNA Expression (RNAseq, CCLE)
Copy Number
H
AR proficient
AR deficient
RWPE-1
RWPE-2
WPE-NB14
LNCaP
VCaP
CA-HPV-10
DU145
PC3
22Rv1
ARF1
ARF6
IQSEC1
GAPDH
I
IQSEC1 expression
Normal
Tumour
J
Quartiles
IQSEC1
Biochemical Relapse-free Survival
Time (d)

Fig 1

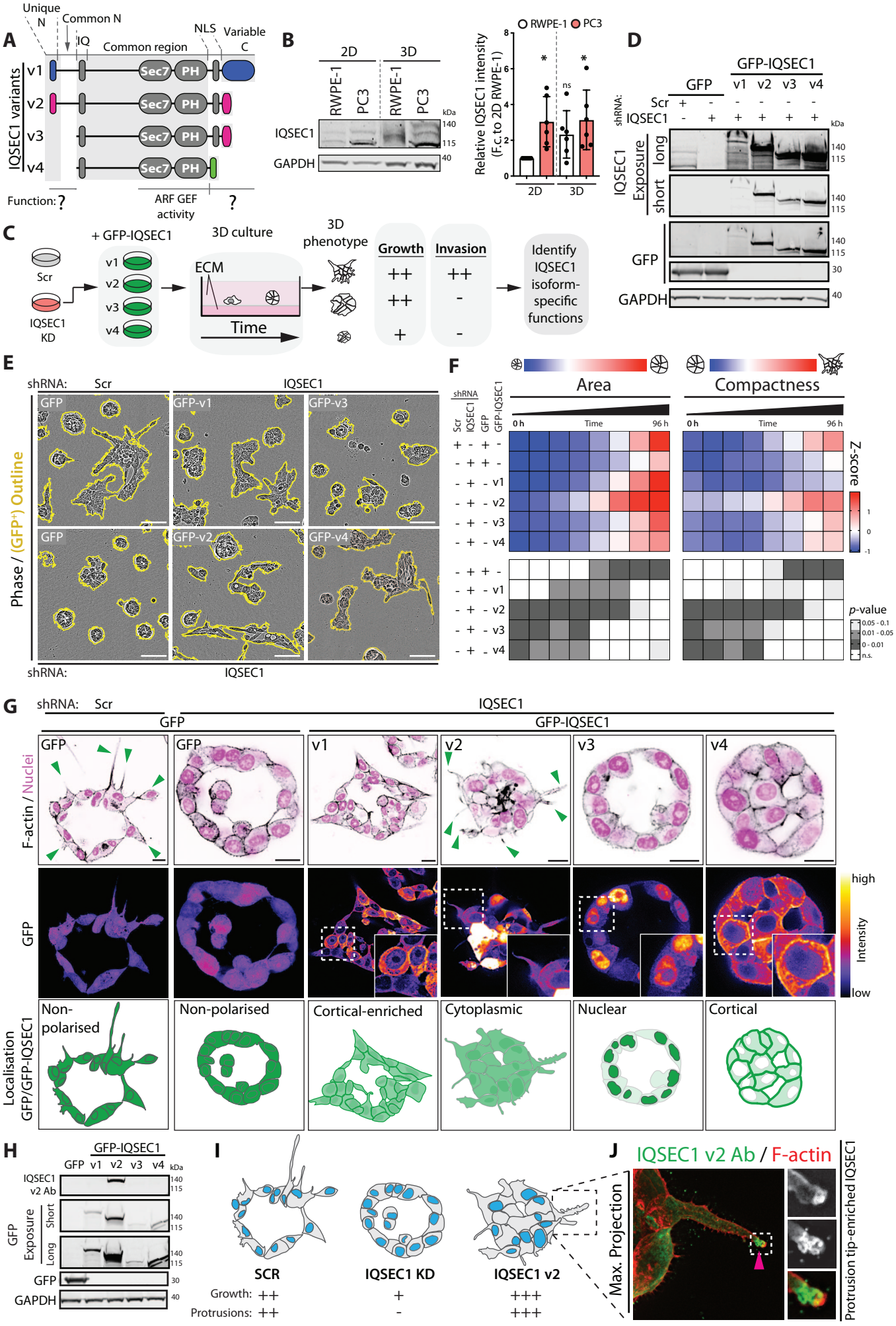
A
Unique N
Common N
IQ
Common region
NLS
Variable C
IQSEC1 variants
v1
v2
v3
v4
Sec7
PH
Function: ?
ARF GEF activity
?
B
2D
3D
RWPE-1
PC3
RWPE-1
PC3
kDa
IQSEC1
GAPDH
140
115
40
RWPE-1
PC3
Relative IQSEC1 intensity (F.c. to 2D RWPE-1)
ns
2D
3D
D
GFP-IQSEC1
GFP
v1 v2 v3 v4
shRNA:
Scr
IQSEC1
IQSEC1
Exposure
long
short
GFP
GAPDH
30
40
C
+ GFP-IQSEC1
3D culture
3D phenotype
Scr
IQSEC1 KD
v1
v2
v3
v4
ECM
Time
Growth
Invasion
++
++
+
++
-
-
Identify IQSEC1 isoform-specific functions
E
shRNA:
Scr
IQSEC1
GFP
GFP-v1
GFP-v3
GFP-v2
GFP-v4
Phase / (GFP+) Outline
F
Area
Compactness
shRNA
Scr
IQSEC1
GFP
GFP-IQSEC1
0 h
Time
96 h
Z-score
p-value
0.05 - 0.1
0.01 - 0.05
0 - 0.01
n.s.
G
shRNA:
Scr
IQSEC1
GFP
GFP-IQSEC1
F-actin / Nuclei
GFP
v1
v2
v3
v4
high
Intensity
low
Localisation GFP/GFP-IQSEC1
Non-polarised
Non-polarised
Cortical-enriched
Cytoplasmic
Nuclear
Cortical
H
GFP-IQSEC1
GFP v1 v2 v3 v4
kDa
IQSEC1 v2 Ab
GFP Exposure
Short
Long
GFP
GAPDH
140
115
30
40
I
SCR
IQSEC1 KD
IQSEC1 v2
Growth: ++
Protrusions: ++
+
-
+++
+++
J
IQSEC1 v2 Ab / F-actin
Max. Projection
Protrusion tip-enriched IQSEC1

Fig 2

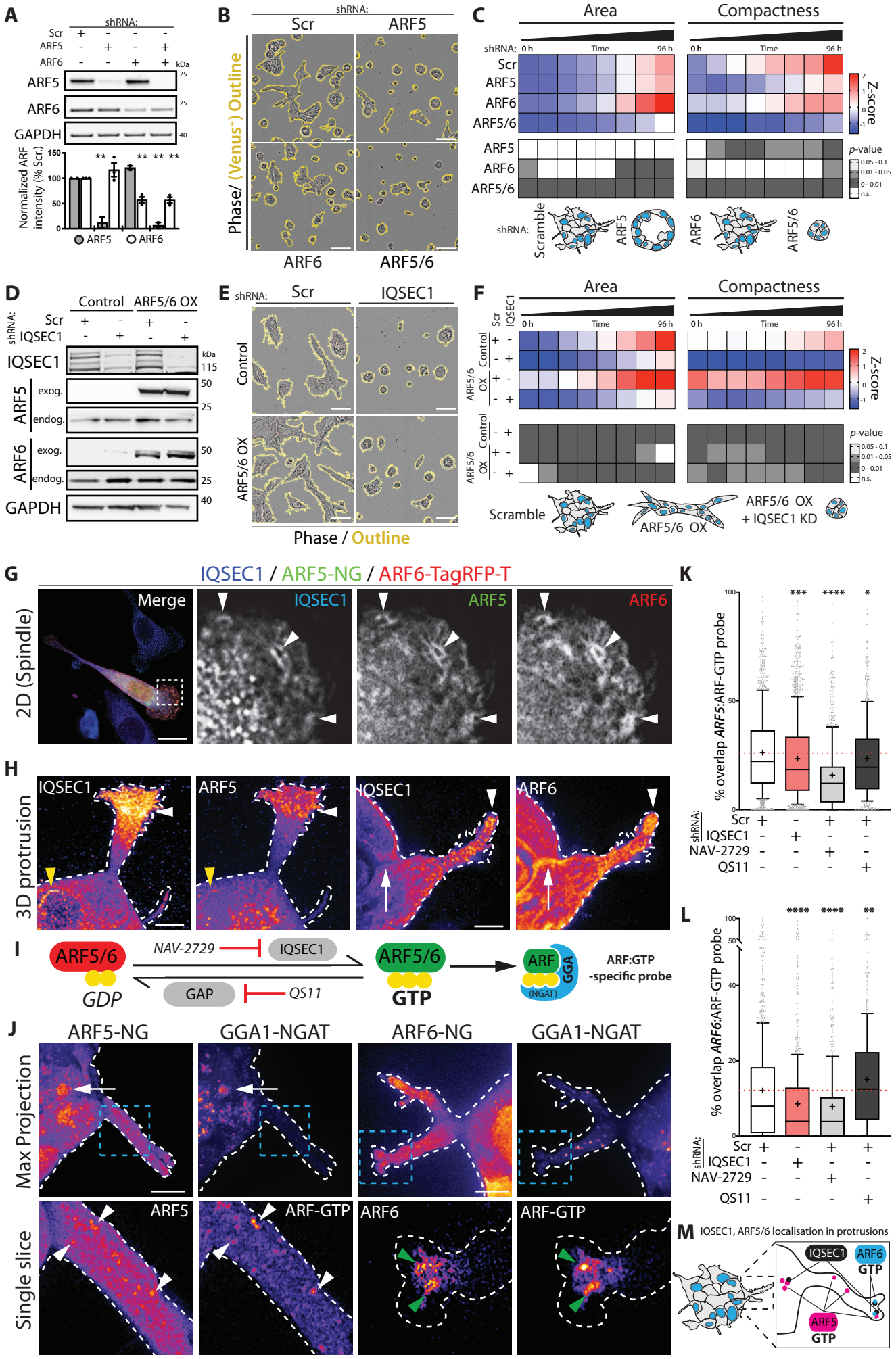
A
shRNA:
Scr
ARF5
ARF6
kDa
GAPH
Normalized ARF intensity (% Scr.)
ARF5
ARF6
B
shRNA:
Scr
ARF5
Phase/ (Venus+) Outline
ARF6
ARF5/6
C
Area
Compactness
shRNA:
0 h
Time
96 h
Scr
ARF5
ARF6
ARF5/6
Z-score
p-value
0.05 - 0.1
0.01 - 0.05
0 - 0.01
n.s.
Scramble
ARF5
ARF6
ARF5/6
D
Control
ARF5/6 OX
shRNA:
Scr
IQSEC1
IQSEC1
ARF5
exog.
endog.
ARF6
exog.
endog.
GAPH
E
shRNA:
Scr
IQSEC1
Control
ARF5/6 OX
Phase / Outline
F
Area
Compactness
Scr
IQSEC1
0 h
Time
96 h
ARF5/6
Control
OX
Z-score
p-value
Scramble
ARF5/6 OX
ARF5/6 OX
+ IQSEC1 KD
G
IQSEC1 / ARF5-NG / ARF6-TagRFP-T
2D (Spindle)
Merge
IQSEC1
ARF5
ARF6
H
3D protrusion
IQSEC1
ARF5
IQSEC1
ARF6
I
ARF5/6
GDP
NAV-2729
IQSEC1
GAP
QS11
ARF5/6
GTP
ARF
GGA
(NGAT)
ARF:GTP
-specific probe
J
ARF5-NG
GGA1-NGAT
ARF6-NG
GGA1-NGAT
Max Projection
Single slice
ARF5
ARF-GTP
ARF6
ARF-GTP
K
% overlap ARF5:ARF-GTP probe
shRNA:
Scr
IQSEC1
NAV-2729
QS11
L
% overlap ARF6:ARF-GTP probe
shRNA:
Scr
IQSEC1
NAV-2729
QS11
M
IQSEC1, ARF5/6 localisation in protrusions
IQSEC1
ARF6
GTP
ARF5
GTP

Fig 3

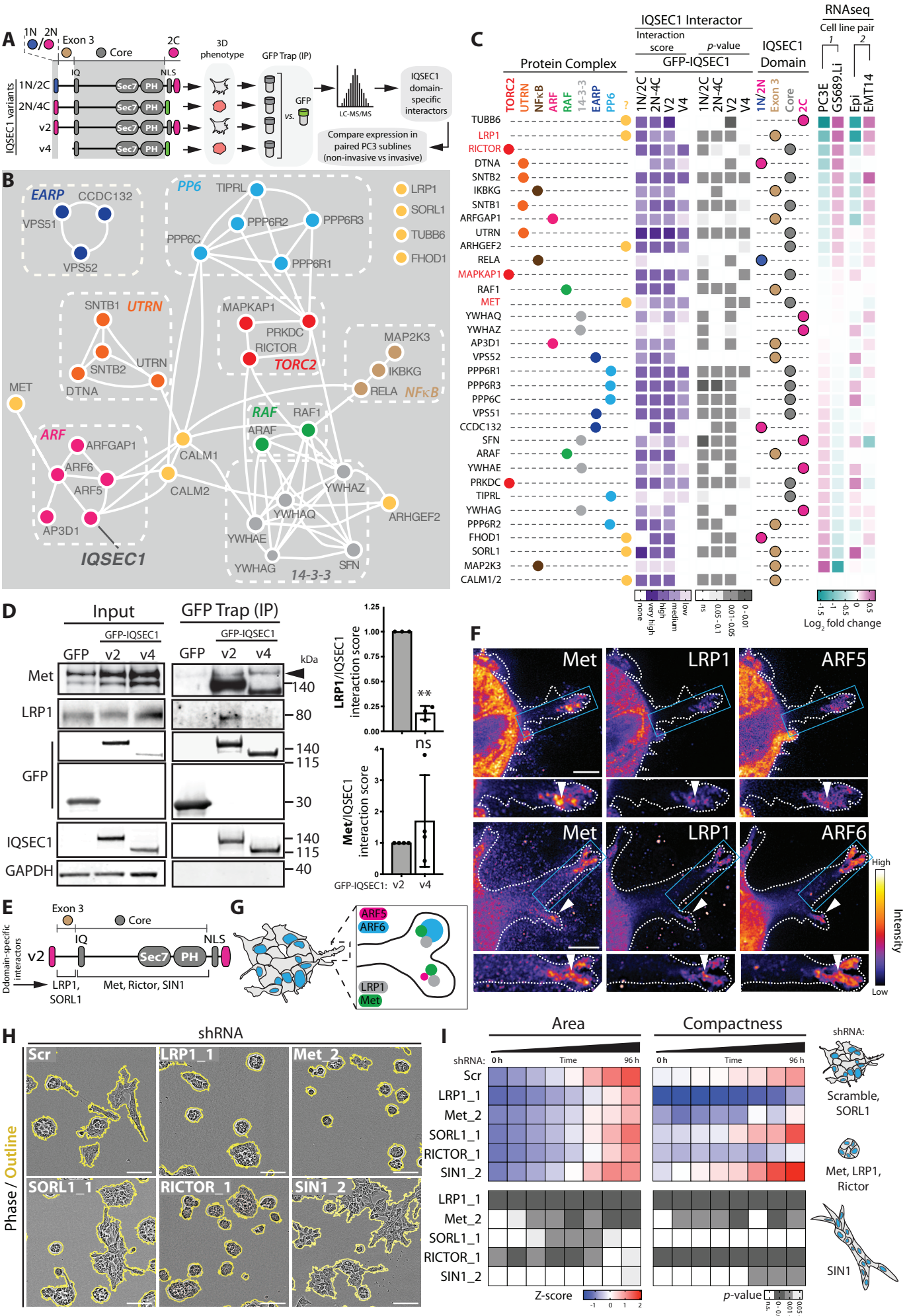
A
1N 2N
Exon 3
Core
2C
IQ
NLS
IQSEC1 variants
1N/2C
2N/4C
v2
v4
Sec7
PH
3D phenotype
GFP Trap (IP)
GFP
vs.
LC-MS/MS
IQSEC1 domain-specific interactors
Compare expression in paired PC3 sublines (non-invasive vs invasive)
B
EARP
CCDC132
VPS51
VPS52
PP6
TIPRL
PPP6R2
PPP6R3
PPP6C
PPP6R1
LRP1
SORL1
TUBB6
FHOD1
SNTB1
UTRN
SNTB2
DTNA
MAPKAP1
PRKDC
RICTOR
TORC2
MAP2K3
IKBKG
RELA
NFκB
MET
RAF
RAF1
ARAF
ARF
ARFGAP1
ARF6
ARF5
AP3D1
IQSEC1
CALM1
CALM2
YWHAZ
YWHAQ
YWHAE
YWHAG
14-3-3
SFN
ARHGEF2
C
Protein Complex
IQSEC1 Interactor
Interaction score
p-value
GFP-IQSEC1
IQSEC1 Domain
RNAseq
Cell line pair
1
2
TORC2
UTRN
NFκB
ARF
RAF
14-3-3
EARP
PP6
?
1N/2C
2N-4C
V2
V4
1N/2N
Exon 3
Core
2C
PC3E
GS689.Li
Epi
EMT14
TUBB6
LRP1
RICTOR
DTNA
SNTB2
IKBKG
SNTB1
ARFGAP1
UTRN
ARHGEF2
RELA
MAPKAP1
RAF1
MET
YWHAQ
YWHAZ
AP3D1
VPS52
PPP6R1
PPP6R3
PPP6C
VPS51
CCDC132
SFN
ARAF
YWHAE
PRKDC
TIPRL
YWHAG
PPP6R2
FHOD1
SORL1
MAP2K3
CALM1/2
none
very high
high
medium
low
ns
0.05 - 0.1
0.01 - 0.05
0 - 0.01
-1.5
-1
-0.5
0
0.5
Log2 fold change
D
Input
GFP Trap (IP)
GFP-IQSEC1
GFP
v2
v4
kDa
Met
LRP1
GFP
IQSEC1
GAPDH
140
80
140
115
30
140
115
40
LRP1/IQSEC1 interaction score
1.25
1.00
0.75
0.50
0.25
0.00
**
ns
Met/IQSEC1 interaction score
4
3
2
1
0
GFP-IQSEC1: v2 v4
E
Exon 3
Core
IQ
NLS
v2
Sec7
PH
Ddomain-specific interactors
LRP1, SORL1
Met, Rictor, SIN1
G
ARF5
ARF6
LRP1
Met
F
Met
LRP1
ARF5
ARF6
High
Intensity
Low
H
shRNA
Scr
LRP1_1
Met_2
SORL1_1
RICTOR_1
SIN1_2
Phase / Outline
I
Area
Compactness
shRNA:
0 h
Time
96 h
Scr
LRP1_1
Met_2
SORL1_1
RICTOR_1
SIN1_2
Z-score
-1
0
1
2
p-value
n.s.
0 - 0.01
0.01 - 0.05
0.05 - 0.1
Scramble, SORL1
Met, LRP1, Rictor
SIN1

Fig 4

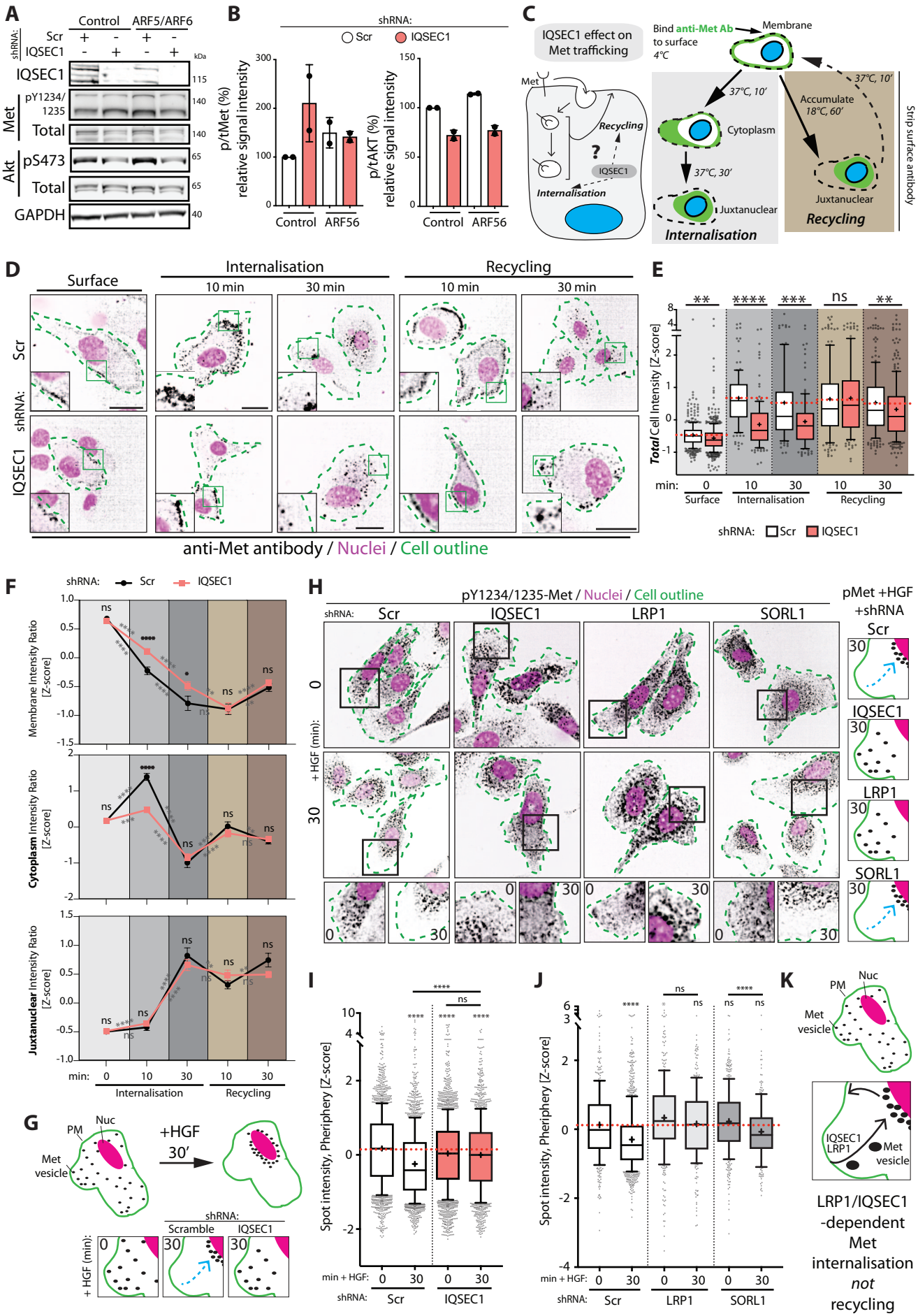
A
Control
ARF5/ARF6
shRNA:
Scr
IQSEC1
kDa
IQSEC1
Met
pY1234/1235
Total
Akt
pS473
Total
GAPDH
B
shRNA:
Scr
IQSEC1
p/tMet (%) relative signal intensity
p/tAKT (%) relative signal intensity
Control
ARF56
C
IQSEC1 effect on Met trafficking
Met
Recycling
IQSEC1
Internalisation
Bind anti-Met Ab to surface 4°C
Membrane
37°C, 10'
Cytoplasm
37°C, 30'
Juxtanuclear
Internalisation
37°C, 10'
Accumulate 18°C, 60'
Juxtanuclear
Recycling
Strip surface antibody
D
Surface
Internalisation
Recycling
10 min
30 min
Scr
shRNA:
IQSEC1
anti-Met antibody / Nuclei / Cell outline
E
Total Cell Intensity [Z-score]
min:
Surface
Internalisation
Recycling
shRNA:
Scr
IQSEC1
F
shRNA:
Scr
IQSEC1
Membrane Intensity Ratio [Z-score]
Cytoplasm Intensity Ratio [Z-score]
Juxtanuclear Intensity Ratio [Z-score]
min:
Internalisation
Recycling
G
PM
Nuc
Met vesicle
+HGF 30'
shRNA:
Scramble
IQSEC1
+ HGF (min):
H
pY1234/1235-Met / Nuclei / Cell outline
shRNA:
Scr
IQSEC1
LRP1
SORL1
+ HGF (min):
pMet +HGF +shRNA
I
Spot intensity, Pheriphery [Z-score]
min + HGF:
shRNA:
Scr
IQSEC1
J
Spot intensity, Pheriphery [Z-score]
min + HGF:
shRNA:
Scr
LRP1
SORL1
K
PM
Nuc
Met vesicle
IQSEC1
LRP1
Met vesicle
LRP1/IQSEC1 -dependent Met internalisation *not* recycling

Fig 5

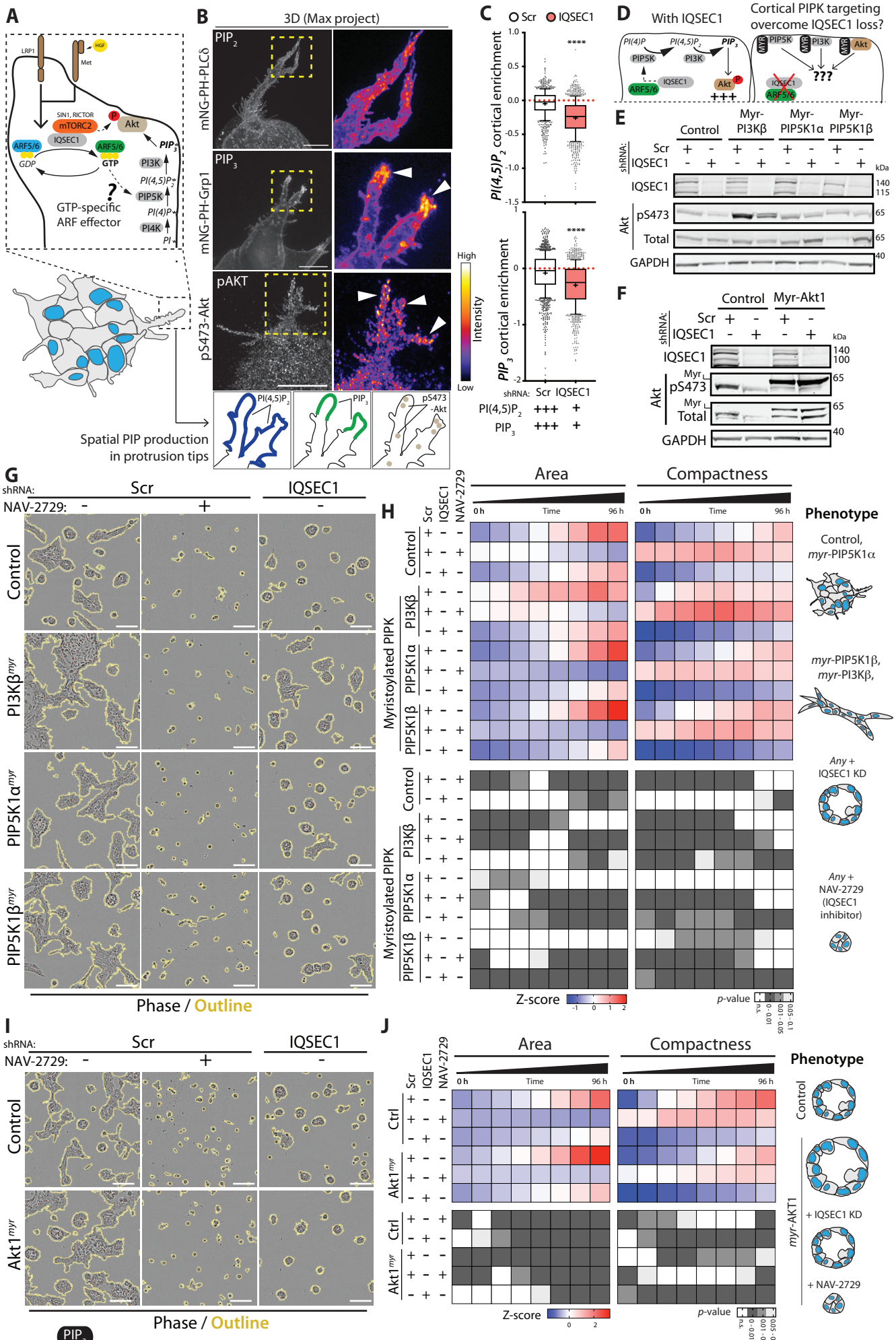
A
LRP1
HGF
Met
SIN1, RICTOR
mTORC2
Akt
IQSEC1
ARF5/6
GDP
GTP
PIP3
PI3K
PI(4,5)P2
PIP5K
PI(4)P
PI4K
PI
GTP-specific
ARF effector
Spatial PIP production
in protrusion tips
B
3D (Max project)
mNG-PH-PLCδ
mNG-PH-Grp1
pAKT
pS473-Akt
High
Intensity
Low
PI(4,5)P2
PIP3
pS473
-Akt
C
Scr
IQSEC1
PI(4,5)P2 cortical enrichment
PIP3 cortical enrichment
****
shRNA: Scr IQSEC1
PI(4,5)P2 +++ +
PIP3 +++ +
D
With IQSEC1
Cortical PIPK targeting
overcome IQSEC1 loss?
PI(4)P
PI(4,5)P2
PIP3
PIP5K
PI3K
IQSEC1
ARF5/6
Akt
+++
MYR
???
E
Control
Myr-PI3Kβ
Myr-PIP5K1α
Myr-PIP5K1β
shRNA:
Scr
IQSEC1
kDa
IQSEC1
Akt
pS473
Total
GAPDH
140
115
65
65
40
F
Control
Myr-Akt1
shRNA:
Scr
IQSEC1
kDa
IQSEC1
Akt
Myr
pS473
Myr
Total
GAPDH
140
100
65
65
40
G
shRNA:
Scr
IQSEC1
NAV-2729:
-
+
-
Control
PI3Kβmyr
PIP5K1αmyr
PIP5K1βmyr
Phase / Outline
H
Scr
IQSEC1
NAV-2729
Area
Compactness
0 h
Time
96 h
Control
PI3Kβ
PIP5K1α
PIP5K1β
Myristoylated PIPK
Phenotype
Control,
myr-PIP5K1α
myr-PIP5K1β,
myr-PI3Kβ,
Any +
IQSEC1 KD
Any +
NAV-2729
(IQSEC1
inhibitor)
Z-score
-1
0
1
2
p-value
n.s.
0 - 0.01
0.01 - 0.05
0.05 - 0.1
I
shRNA:
Scr
IQSEC1
NAV-2729:
-
+
-
Control
Akt1myr
Phase / Outline
J
Scr
IQSEC1
NAV-2729
Area
Compactness
0 h
Time
96 h
Ctrl
Akt1myr
Phenotype
Control
myr-AKT1
+ IQSEC1 KD
+ NAV-2729
Z-score
0
2
p-value
n.s.
0 - 0.01
0.01 - 0.05
0.05 - 0.1
K
PIP3
cortical level
& location:
Low
High
High
2D phenotype
Symmetric
Cortically
restricted
Protrusion-
enriched
Symmetric
Asymmetric
3D phenotype
Outcome:
Round
Spread
Spindle
Growth, no invasion
Invasion & growth
Restriction of
Met-driven PIP3
production
to protrusions
by IQSEC1 v2

Fig 6

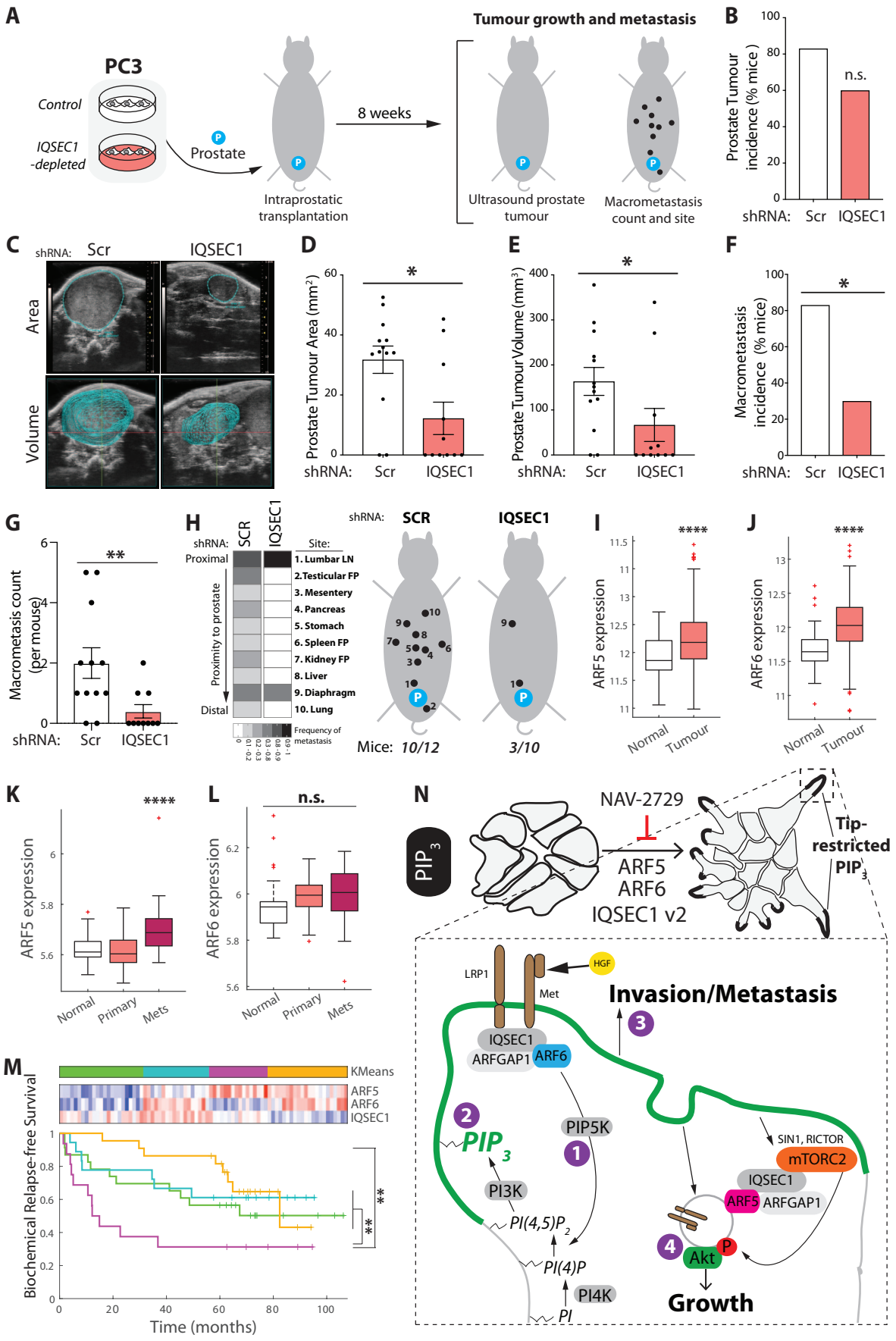
A
PC3
Control
IQSEC1 -depleted
Prostate
Intraprostatic transplantation
8 weeks
Tumour growth and metastasis
Ultrasound prostate tumour
Macrometastasis count and site
B
Prostate Tumour incidence (% mice)
n.s.
shRNA: Scr IQSEC1
C
shRNA: Scr IQSEC1
Area
Volume
D
Prostate Tumour Area (mm²)
shRNA: Scr IQSEC1
E
Prostate Tumour Volume (mm³)
shRNA: Scr IQSEC1
F
Macrometastasis incidence (% mice)
shRNA: Scr IQSEC1
G
Macrometasis count (per mouse)
shRNA: Scr IQSEC1
H
shRNA: SCR IQSEC1
Proximal
Distal
Proximity to prostate
Site:
1. Lumbar LN
2. Testicular FP
3. Mesentery
4. Pancreas
5. Stomach
6. Spleen FP
7. Kidney FP
8. Liver
9. Diaphragm
10. Lung
Frequency of metastasis
Mice: 10/12
3/10
I
ARF5 expression
Normal
Tumour
J
ARF6 expression
Normal
Tumour
K
ARF5 expression
Normal
Primary
Mets
L
n.s.
ARF6 expression
Normal
Primary
Mets
M
KMeans
ARF5
ARF6
IQSEC1
Biochemical Relapse-free Survival
Time (months)
N
PIP3
NAV-2729
ARF5
ARF6
IQSEC1 v2
Tip-restricted PIP3
LRP1
HGF
Met
Invasion/Metastasis
IQSEC1
ARFGAP1
ARF6
PIP5K
PIP3
PI3K
PI(4,5)P2
PI(4)P
PI4K
PI
SIN1, RICTOR
mTORC2
IQSEC1
ARF5
ARFGAP1
Akt
P
Growth

Fig 7

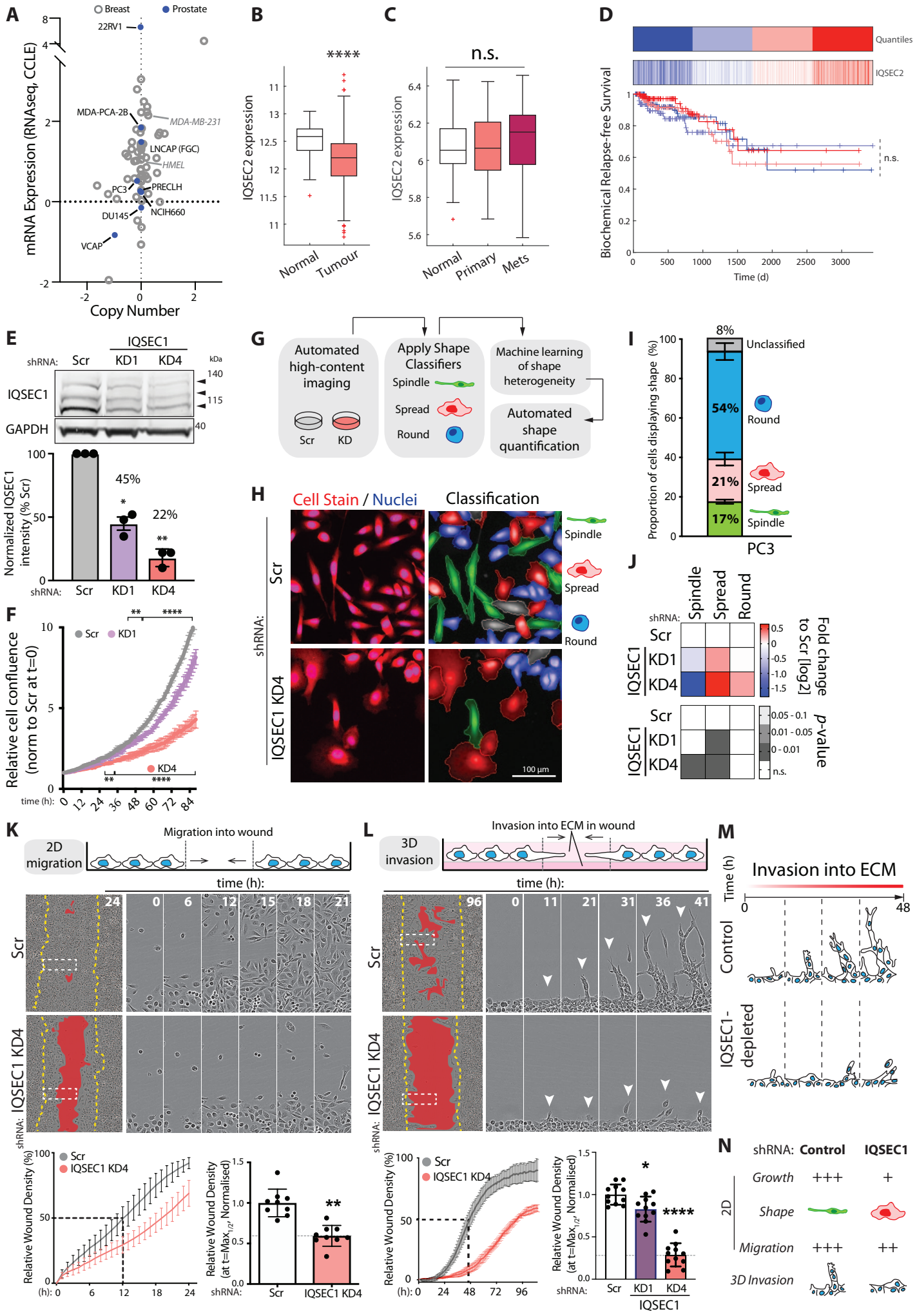
A
Breast
Prostate
22RV1
MDA-PCA-2B
MDA-MB-231
LNCAP (FGC)
HMEL
PC3
PRECLH
DU145
NCIH660
VCAP
mRNA Expression (RNAseq, CCLE)
Copy Number
B
****
IQSEC2 expression
Normal
Tumour
C
n.s.
IQSEC2 expression
Normal
Primary
Mets
D
Quantiles
IQSEC2
Biochemical Relapse-free Survival
n.s.
Time (d)
E
IQSEC1
shRNA: Scr KD1 KD4
kDa
IQSEC1
GAPDH
140
115
40
Normalized IQSEC1 intensity (% Scr)
45%
22%
shRNA: Scr KD1 KD4
F
Scr
KD1
KD4
Relative cell confluence (norm to Scr at t=0)
time (h):
G
Automated high-content imaging
Scr KD
Apply Shape Classifiers
Spindle
Spread
Round
Machine learning of shape heterogeneity
Automated shape quantification
H
Cell Stain / Nuclei
Classification
shRNA:
Scr
IQSEC1 KD4
Spindle
Spread
Round
100 µm
I
Proportion of cells displaying shape (%)
8%
Unclassified
54%
Round
21%
Spread
17%
Spindle
PC3
J
Spindle
Spread
Round
shRNA:
Scr
IQSEC1
KD1
KD4
Fold change to Scr [log2]
p-value
0.05 - 0.1
0.01 - 0.05
0 - 0.01
n.s.
K
2D migration
Migration into wound
time (h):
Scr
IQSEC1 KD4
shRNA:
Relative Wound Density (%)
Relative Wound Density (at t=Max1/2, Normalised)
L
3D invasion
Invasion into ECM in wound
time (h):
Scr
IQSEC1 KD4
shRNA:
Relative Wound Density (%)
Relative Wound Density (at t=Max1/2, Normalised)
M
Invasion into ECM
Time (h)
Control
IQSEC1-depleted
N
shRNA: Control IQSEC1
2D
Growth +++ +
Shape
Migration +++ ++
3D Invasion

SFig 1

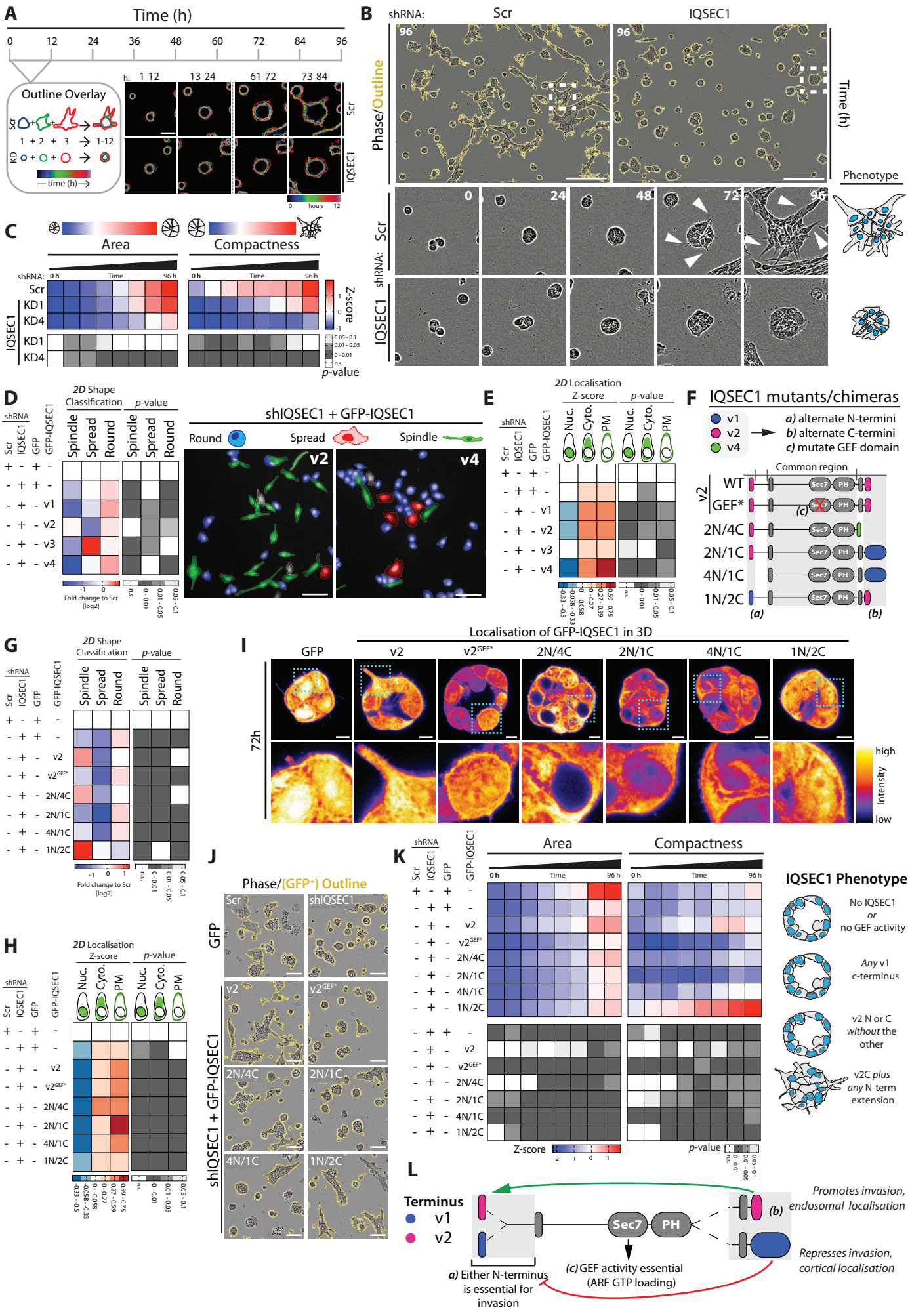
A
Time (h)
Outline Overlay
B
shRNA:
Scr
IQSEC1
Phase/Outline
Time (h)
Phenotype
C
Area
Compactness
Z-score
p-value
D
2D Shape Classification
p-value
shIQSEC1 + GFP-IQSEC1
Round
Spread
Spindle
E
2D Localisation
Z-score
F
IQSEC1 mutants/chimeras
a) alternate N-termini
b) alternate C-termini
c) mutate GEF domain
Common region
G
H
I
Localisation of GFP-IQSEC1 in 3D
72h
high
Intensity
low
J
Phase/(GFP+) Outline
shIQSEC1 + GFP-IQSEC1
K
IQSEC1 Phenotype
No IQSEC1 or no GEF activity
Any v1 c-terminus
v2 N or C without the other
v2C plus any N-term extension
L
Terminus
Promotes invasion, endosomal localisation
Represses invasion, cortical localisation
a) Either N-terminus is essential for invasion
(c) GEF activity essential (ARF GTP loading)

SFig 2

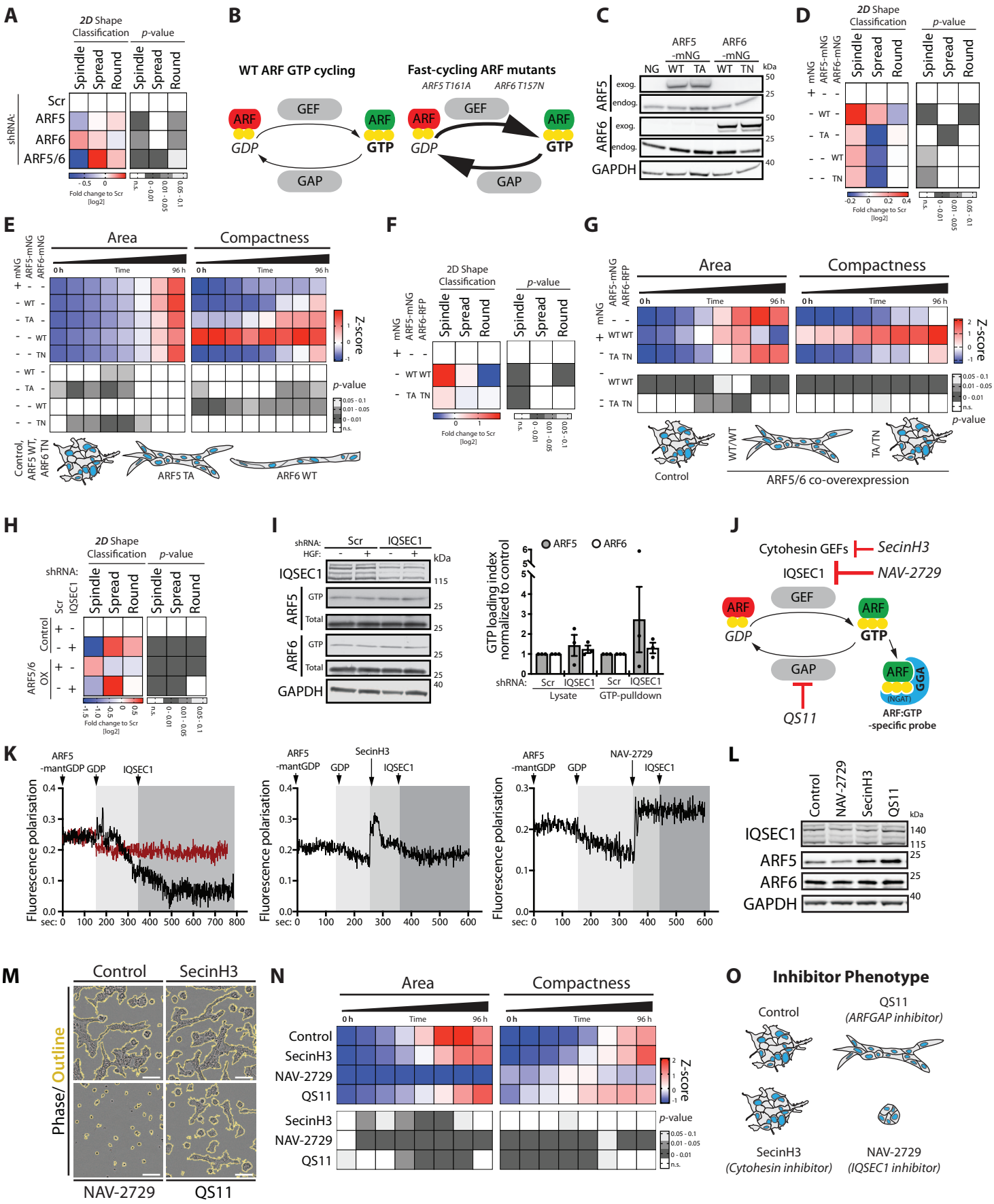
A
2D Shape Classification
p-value
Spindle
Spread
Round
shRNA:
Scr
ARF5
ARF6
ARF5/6
Fold change to Scr [log2]
B
WT ARF GTP cycling
Fast-cycling ARF mutants
ARF5 T161A
ARF6 T157N
ARF
GDP
GTP
GEF
GAP
C
ARF5 -mNG
ARF6 -mNG
NG
WT
TA
TN
kDa
exog.
endog.
GAPDH
D
mNG
ARF5-mNG
ARF6-mNG
E
Area
Compactness
0 h
Time
96 h
Z-score
p-value
Control, ARF5 WT, ARF6 TN
ARF5 TA
ARF6 WT
F
ARF5-mNG
ARF6-RFP
G
Control
WT/WT
TA/TN
ARF5/6 co-overexpression
H
ARF5/6 OX
I
IQSEC1
HGF:
GTP
Total
GTP loading index normalized to control
ARF5
ARF6
Lysate
GTP-pulldown
J
Cytohesin GEFs
SecinH3
NAV-2729
QS11
GGA
(NGAT)
ARF:GTP -specific probe
K
ARF5 -mantGDP
GDP
IQSEC1
SecinH3
NAV-2729
Fluorescence polarisation
sec:
L
Control
NAV-2729
SecinH3
QS11
M
Phase/ Outline
N
O
Inhibitor Phenotype
QS11 (ARFGAP inhibitor)
SecinH3 (Cytohesin inhibitor)
NAV-2729 (IQSEC1 inhibitor)

SFig 3

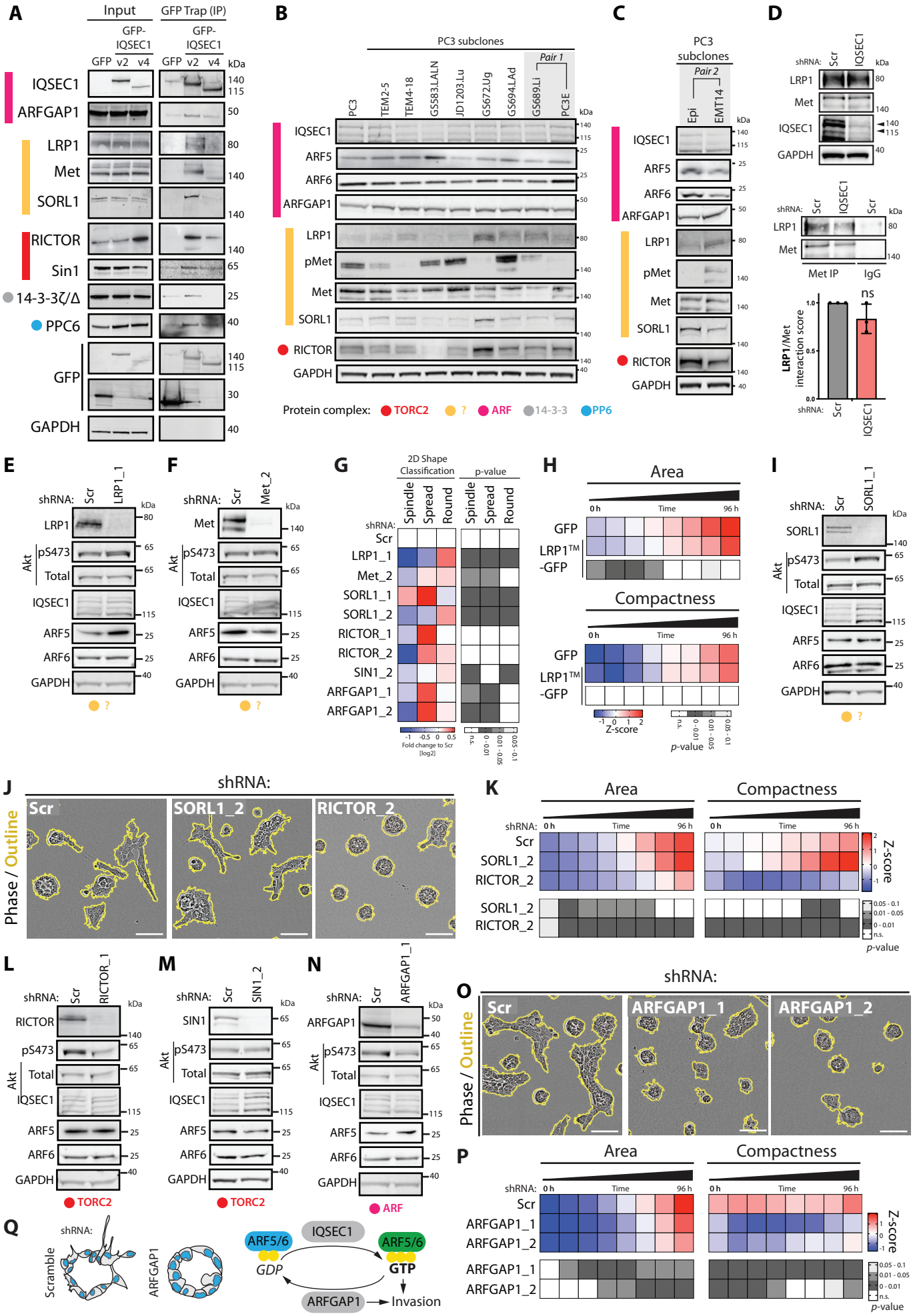
A
Input
GFP Trap (IP)
GFP-IQSEC1
GFP v2 v4
kDa
IQSEC1
ARFGAP1
LRP1
Met
SORL1
RICTOR
Sin1
14-3-3ζ/Δ
PPC6
GFP
GAPDH
B
PC3 subclones
PC3
TEM2-5
TEM4-18
GS583.LALN
JD1203.Lu
GS672.Ug
GS694.Lad
GS689.Li
PC3E
Pair 1
IQSEC1
ARF5
ARF6
ARFGAP1
LRP1
pMet
Met
SORL1
RICTOR
GAPDH
Protein complex: TORC2 ? ARF 14-3-3 PP6
C
PC3 subclones
Pair 2
Epi
EMT14
D
shRNA: Scr IQSEC1
LRP1
Met
IQSEC1
GAPDH
Met IP
IgG
LRP1/Met interaction score
ns
E
shRNA: Scr LRP1_1
LRP1
Akt
pS473
Total
IQSEC1
ARF5
ARF6
GAPDH
F
shRNA: Scr Met_2
Met
G
2D Shape Classification
p-value
Spindle
Spread
Round
shRNA:
Scr
LRP1_1
Met_2
SORL1_1
SORL1_2
RICTOR_1
RICTOR_2
SIN1_2
ARFGAP1_1
ARFGAP1_2
Fold change to Scr [log2]
H
Area
Time
0 h
96 h
GFP
LRP1™-GFP
Compactness
Z-score
p-value
I
shRNA: Scr SORL1_1
SORL1
J
shRNA:
Scr
SORL1_2
RICTOR_2
Phase / Outline
K
Area
Compactness
L
shRNA: Scr RICTOR_1
RICTOR
M
shRNA: Scr SIN1_2
SIN1
N
shRNA: Scr ARFGAP1_1
ARFGAP1
TORC2
ARF
O
shRNA:
Scr
ARFGAP1_1
ARFGAP1_2
P
Q
shRNA:
Scramble
ARFGAP1
ARF5/6
IQSEC1
GDP
GTP
ARFGAP1
Invasion

SFig 4

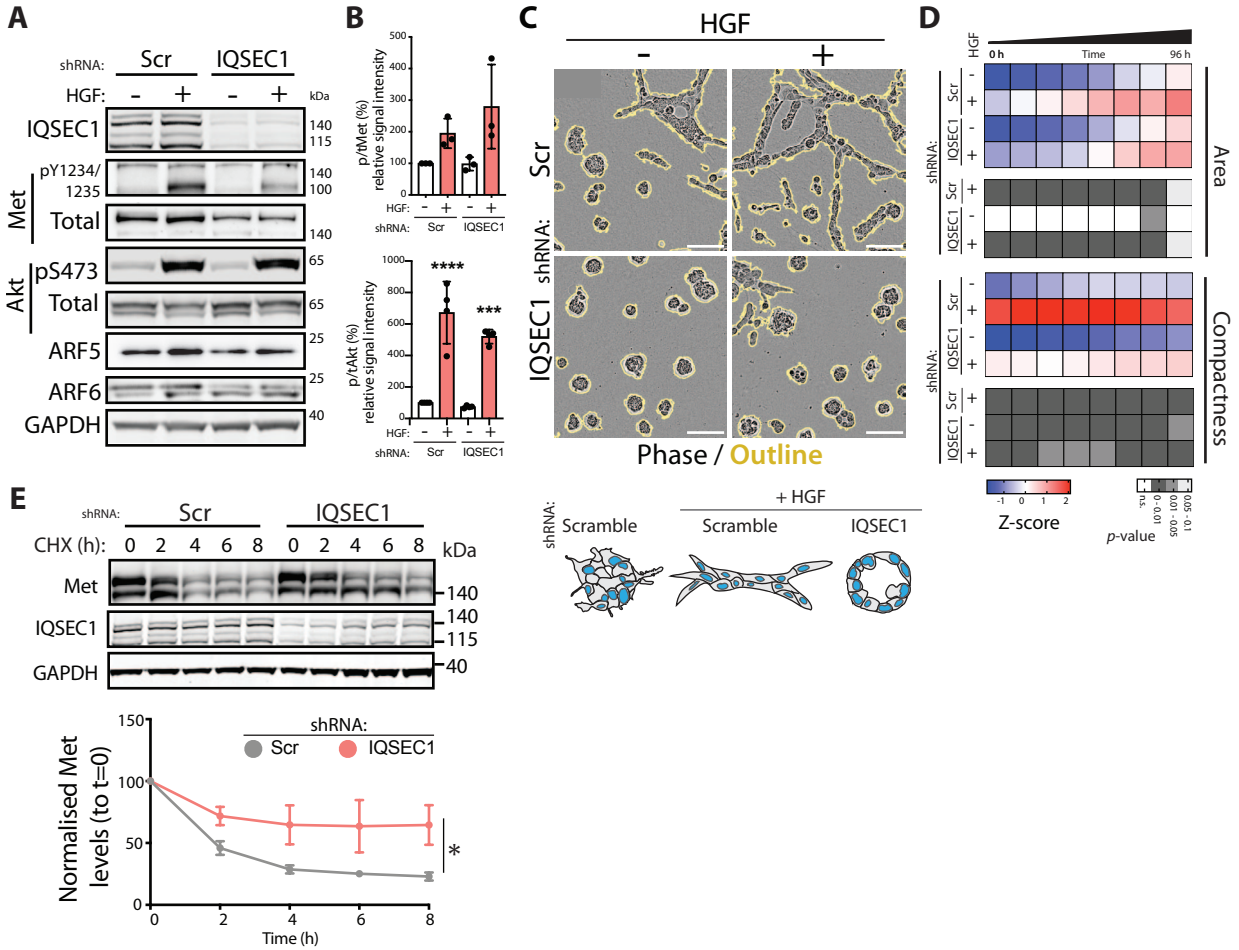
A
shRNA: Scr IQSEC1
HGF: - + - +
kDa
IQSEC1
140
115
Met
pY1234/1235
140
100
Total
140
Akt
pS473
65
Total
65
ARF5
25
ARF6
25
GAPDH
40
B
p/tMet (%) relative signal intensity
p/tAkt (%) relative signal intensity
****
***
HGF: - + - +
shRNA: Scr IQSEC1
C
HGF
-
+
Scr
IQSEC1
shRNA:
Phase / Outline
+ HGF
shRNA:
Scramble
Scramble
IQSEC1
D
HGF
0 h
Time
96 h
shRNA:
Scr
IQSEC1
Area
Compactness
Z-score
p-value
E
shRNA: Scr IQSEC1
CHX (h): 0 2 4 6 8 0 2 4 6 8
kDa
Met
140
IQSEC1
140
115
GAPDH
40
Normalised Met levels (to t=0)
shRNA:
Scr
IQSEC1
Time (h)
*

SFig 5

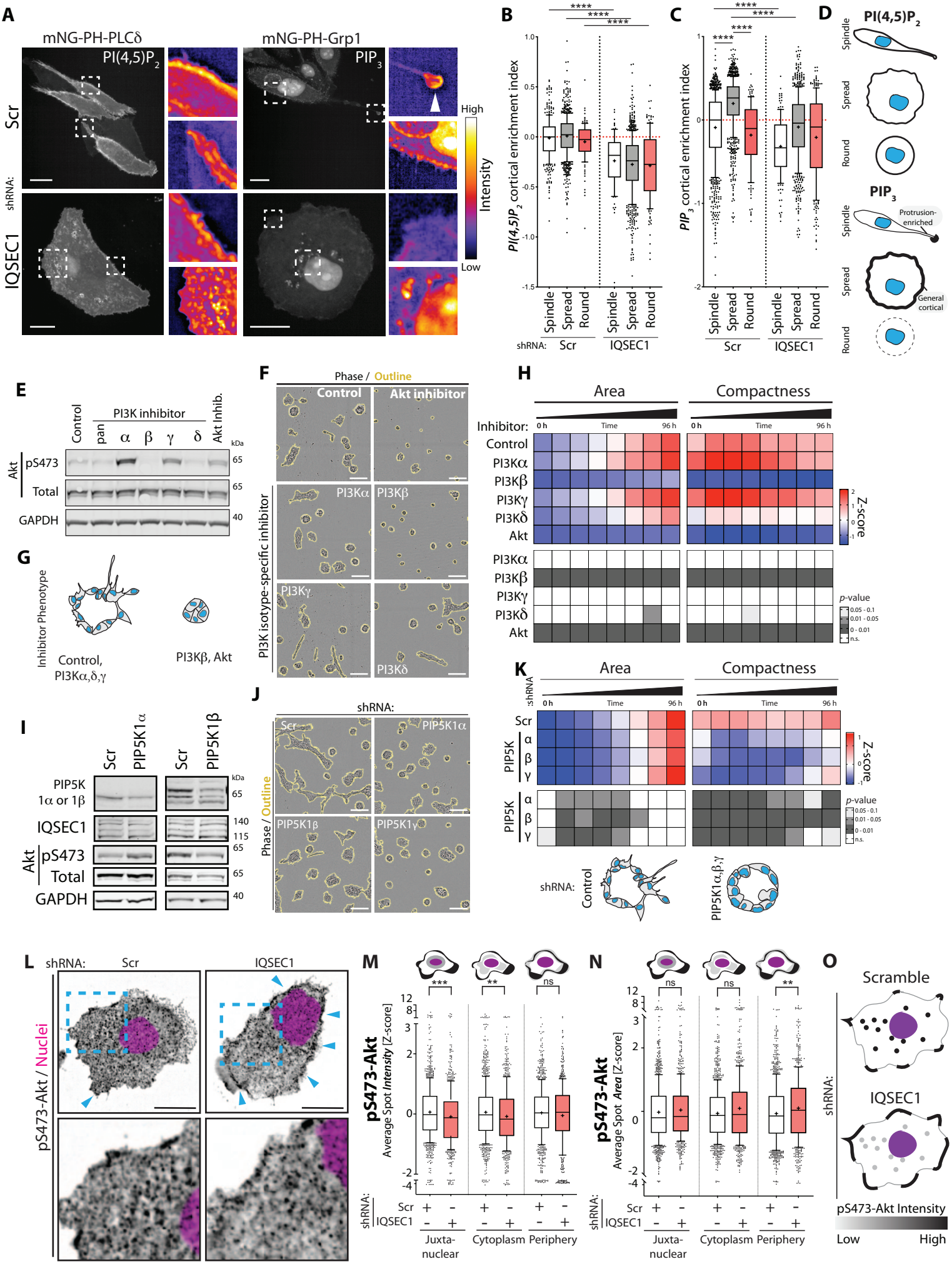
A
mNG-PH-PLCδ
mNG-PH-Grp1
PI(4,5)P2
PIP3
Scr
IQSEC1
shRNA:
High
Intensity
Low
B
PI(4,5)P2 cortical enrichment index
Spindle
Spread
Round
shRNA: Scr IQSEC1
C
PIP3 cortical enrichment index
D
PI(4,5)P2
PIP3
Protrusion-enriched
General cortical
E
Control
PI3K inhibitor
pan α β γ δ
Akt Inhib.
Akt
pS473
Total
GAPDH
kDa
F
Phase / Outline
Control
Akt inhibitor
PI3Kα
PI3Kβ
PI3Kγ
PI3Kδ
PI3K isotype-specific inhibitor
G
Inhibitor Phenotype
Control, PI3Kα,δ,γ
PI3Kβ, Akt
H
Area
Compactness
Inhibitor:
0 h
Time
96 h
Control
PI3Kα
PI3Kβ
PI3Kγ
PI3Kδ
Akt
Z-score
p-value
I
Scr
PIP5K1α
PIP5K1β
PIP5K 1α or 1β
IQSEC1
Akt
pS473
Total
GAPDH
J
shRNA:
Scr
PIP5K1α
PIP5K1β
PIP5K1γ
Phase / Outline
K
shRNA:
PIP5K
α
β
γ
shRNA:
Control
PIP5K1α,β,γ
L
shRNA:
Scr
IQSEC1
pS473-Akt / Nuclei
M
pS473-Akt
Average Spot Intensity [Z-score]
Juxta-nuclear
Cytoplasm
Periphery
N
pS473-Akt
Average Spot Area [Z-score]
O
Scramble
IQSEC1
shRNA:
pS473-Akt Intensity
Low
High

SFig 6

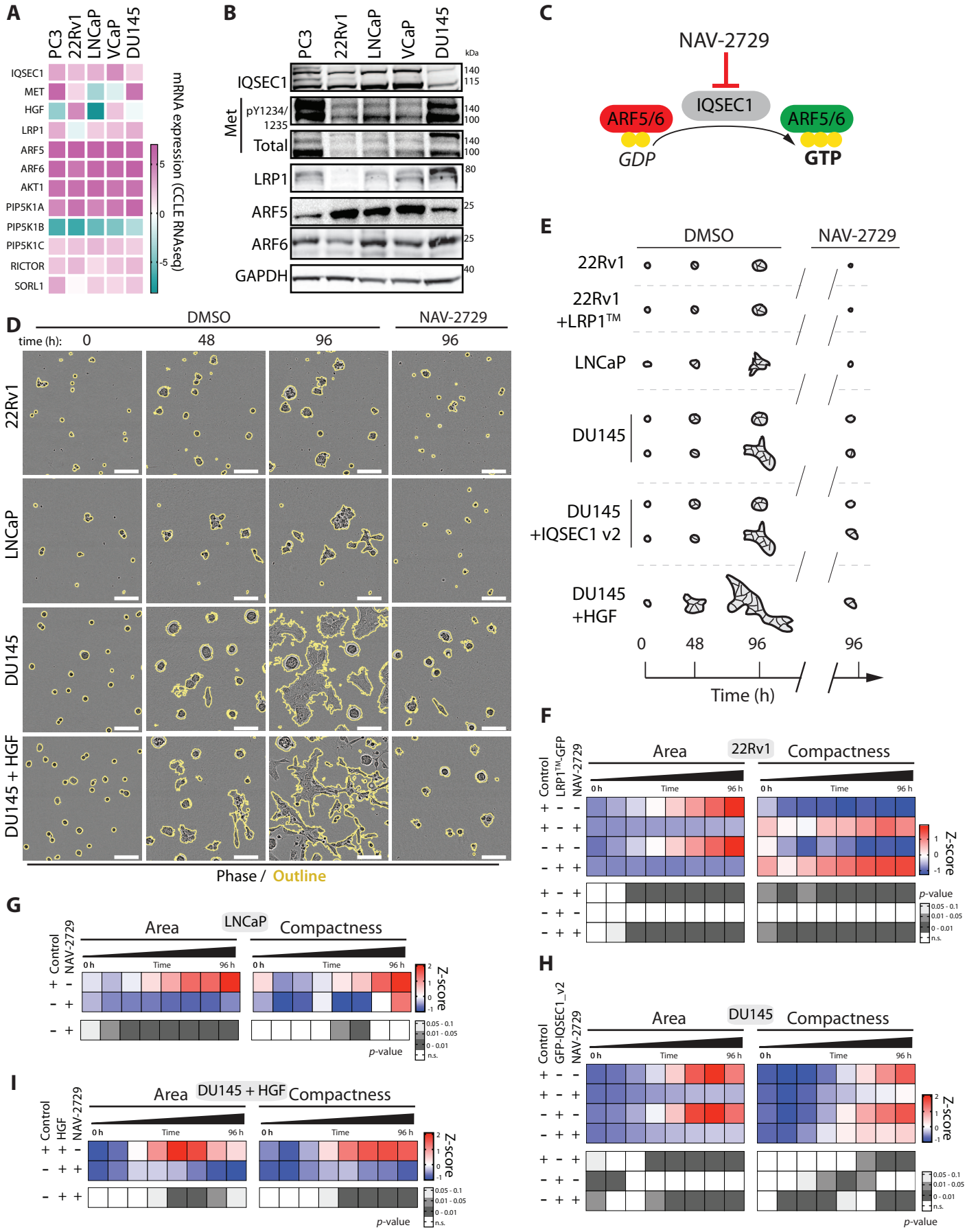
A
PC3
22Rv1
LNCaP
VCaP
DU145
IQSEC1
MET
HGF
LRP1
ARF5
ARF6
AKT1
PIP5K1A
PIP5K1B
PIP5K1C
RICTOR
SORL1
mRNA expression (CCLE RNAseq)
B
kDa
IQSEC1
Met
pY1234/1235
Total
LRP1
ARF5
ARF6
GAPDH
C
NAV-2729
IQSEC1
ARF5/6
GDP
ARF5/6
GTP
D
DMSO
NAV-2729
time (h):
0
48
96
96
22Rv1
LNCaP
DU145
DU145 + HGF
Phase / Outline
E
DMSO
NAV-2729
22Rv1
22Rv1 +LRP1™
LNCaP
DU145
DU145 +IQSEC1 v2
DU145 +HGF
0
48
96
96
Time (h)
F
Area
22Rv1
Compactness
Control
LRP1™-GFP
NAV-2729
0 h
Time
96 h
Z-score
p-value
G
Area
LNCaP
Compactness
Control
NAV-2729
Z-score
p-value
H
Area
DU145
Compactness
Control
GFP-IQSEC1_v2
NAV-2729
Z-score
p-value
I
Area
DU145 + HGF
Compactness
Control
HGF
NAV-2729
Z-score
p-value

SFig 7